

This article was downloaded by: [Cornell University]

On: 18 August 2012, At: 12:20

Publisher: Taylor & Francis

Informa Ltd Registered in England and Wales Registered Number: 1072954 Registered office: Mortimer House, 37-41 Mortimer Street, London W1T 3JH, UK



## Combustion Theory and Modelling

Publication details, including instructions for authors and subscription information:

<http://www.tandfonline.com/loi/tctm20>

### Propagation speed of combustion and invasion waves in stochastic simulations with competitive mixing

A. Y. Klimenko<sup>a</sup> & S. B. Pope<sup>b</sup>

<sup>a</sup> School of Mechanical and Mining Engineering, University of Queensland, 4072, Qld, Australia

<sup>b</sup> Sibley School of Mechanical and Aerospace Engineering, Cornell University, Ithaca, NY, 14853, USA

Version of record first published: 11 Jan 2012

To cite this article: A. Y. Klimenko & S. B. Pope (2012): Propagation speed of combustion and invasion waves in stochastic simulations with competitive mixing, Combustion Theory and Modelling, 16:4, 679-714

To link to this article: <http://dx.doi.org/10.1080/13647830.2011.647091>

PLEASE SCROLL DOWN FOR ARTICLE

Full terms and conditions of use: <http://www.tandfonline.com/page/terms-and-conditions>

This article may be used for research, teaching, and private study purposes. Any substantial or systematic reproduction, redistribution, reselling, loan, sub-licensing, systematic supply, or distribution in any form to anyone is expressly forbidden.

The publisher does not give any warranty express or implied or make any representation that the contents will be complete or accurate or up to date. The accuracy of any instructions, formulae, and drug doses should be independently verified with primary sources. The publisher shall not be liable for any loss, actions, claims, proceedings, demand, or costs or damages whatsoever or howsoever caused arising directly or indirectly in connection with or arising out of the use of this material.

## Propagation speed of combustion and invasion waves in stochastic simulations with competitive mixing

A.Y. Klimenko<sup>a\*</sup> and S.B. Pope<sup>b</sup>

<sup>a</sup>*School of Mechanical and Mining Engineering, University of Queensland, Qld 4072, Australia;*

<sup>b</sup>*Sibley School of Mechanical and Aerospace Engineering, Cornell University, Ithaca, NY 14853, USA*

(Received 10 July 2011; final version received 25 October 2011)

We consider the propagation speeds of steady waves simulated by particles with stochastic motions, properties and mixing (Pope particles). Conventional conservative mixing is replaced by competitive mixing simulating invasion processes or conditions in turbulent premixed flames under the flamelet regime. The effects of finite correlation times for particle velocity are considered and wave propagation speeds are determined for different limiting regimes. The results are validated by stochastic simulations. If the correlation time is short, the model corresponds to the KPP–Fisher equation, which is conventionally used to simulate invasion processes. If the parameters of the simulations are properly selected, the model under consideration is shown to be consistent with existing experimental evidence for propagation speeds of turbulent premixed flames.

**Keywords:** turbulent premixed flames; competitive mixing; propagation speeds

### Nomenclature

$a$	constant
$A$	normalised acceleration
$b$	premixed flame exponent $\approx 0.3$ or $= 2/7$
$C$	constant
$D$	modelling Damkohler number $= 2\tau_*/\tau_m$
$D_e$	effective modelling Damkohler number, see Equation (28)
$Da$	physical Damkohler number
$\mathcal{D}$	diffusion coefficient
$d$	distance in the phase space
$f(x, u)$	joint PDF of $x^*$ and $u^*$ , $f = \langle \psi \rangle = f_0/l_0$
$f_0(u)$	PDF of $u^*$
$g(x, u)$	$= \langle (1 - Y)\psi \rangle$
$\hat{g}(x, u)$	$= g/f$
$\bar{g}(x)$	$= \langle (1 - Y) x \rangle$
$h(x, u)$	$= \langle Y\psi \rangle$
$\hat{h}(x, u)$	$= h/f$
$\bar{h}(x)$	$= \langle Y x \rangle$

---

\*Corresponding author. Email: klimenko@mech.uq.edu.au

$K$	modelling Knudsen number $K = l_p/l_m$
$Ka$	physical Karlovitz number
$l_0$	length of the domain
$l_0$	r.m.s. distance travelled by a particle in the time $\tau_m$
$l_p$	particle spacing $= L/n_p$
$l_t$	dispersion distance
$l_*$	convective length scale $= \tau_* u_*$
$L$	normalised flame width
$n_p$	number of particles
$N$	number of particles in the transition zone
$p$	probability
$q(x)$	function see Equation (76)
$R$	modelling Reynolds number $= \tau_*^2/\tau_p^2$
$Re$	physical Reynolds number
$r$	time-dependent separation distance in the phase space
$S$	non-dimensional propagation speed $= s/u_*$
$s$	propagation speed of a flame or wave
$s_L$	laminar flame propagation speed
$s_{min}$	minimal propagation speed
$T$	non-dimensional time $= 2\omega_c t$
$t$	time
$U$	non-dimensional sample-space velocity $= u/u_*$
$u$	velocity
$u_{max}$	effective maximal particle velocity
$u^*$	particle velocity
$W(Y)$	(chemical) source term
$W$	source of $\hat{g}$ (negative)
$w(t)$	Wiener process
$X$	non-dimensional position $= 2x\omega_*/u_*$
$x^*$	particle position
$Y$	particle composition
$Z$	non-dimensional front coordinate $Z = (X - ST)$
$\Delta$	increment, zone scale or time step (as followed by another symbol)
$\Phi(Y)$	premixed flamelet function
$\psi(x, u)$	fine-grained joint PDF of $x^*$ and $u^*$
$v$	$= (U - S) S$
$\zeta$	$= (Z - Z_0)$
$\tau_*$	velocity relaxation time scale
$\tau_m$	$\omega_m^{-1}$
$\tau_p$	particle convective collision time $= l_p/u_*$
$\tau_r$	reaction time
$\Omega$	$\omega/\omega_c$
$\omega_c$	collision frequency
$\omega_{c0}$	$\omega_c$ for $u = 0$
$\omega_m$	mixing rate
$(\cdot)$	'tilde' indicates a normalised quantity
$(\cdot)_K$	subscript 'K' indicates Kolmogorov scales
$(\cdot)^\circ$	superscript 'o' indicates effective premixed scales
$(\cdot)^{(p)}, (\cdot)^{(q)}$	superscripts indicate particles p and q.
$(\cdot)^{(p)}, (\cdot)^{(s)}$	superscripts indicate primary and secondary particle.

## 1. Introduction

One of the simplest possible stochastic models for emulating the propagation of combustion waves in turbulent premixed combustion was suggested by Pope and Anand [1]. The model utilises Pope particles – this term was suggested by Klimenko and Cleary [2] in the development of the concept of ‘stochastic particles’ introduced by Pope [3]. In the case when the flame fronts are very thin (the flamelet regime), the model can be formulated with the use of non-conservative or competitive mixing [4]. Competitive mixing can be seen as the superposition of conventional conservative mixing followed by the rapid evolution of the particles into the burned state. The unburned state is interpreted as ‘the loser’ and the burned state is ‘the winner’ in this process. The source terms that correspond to this process are similar to the BML (Bray–Moss–Libby) model for premixed turbulent combustion [5]. Stochastic simulations of turbulent combustion [3, 6–11] and premixed flames [12–20] have been repeatedly reviewed in publications.

A source term similar to ones considered in the present work also appears in the convection–diffusion–reaction equation, which was introduced by Fisher [21]. The mathematical theory for this and similar equations was developed by Kolmogorov, Petrovsky and Piskunov (KPP) [22] and this class of equations is also commonly referred to as the KPP equations. The model under consideration here is different from the KPP–Fisher equation because of the finite correlation time of particle velocities considered in the present work; although, as we show in the paper, the KPP–Fisher equation can be recovered when this correlation time tends to zero. The KPP–Fisher equation is linked to a number of stochastic processes that are conventionally used to describe invasions of successful species or genes. Mollison [23] extensively discussed links of the KPP–Fisher equation with the contact distribution process and other stochastic processes. McKean [24] demonstrated that the position of the leading particle in the branching Brownian random walk process is controlled by the KPP–Fisher equation. Blythe and McKane [25] recently reviewed stochastic models related to the approach originated by Fisher [21]. We note here that Pope particles with competitive mixing give an alternative stochastic interpretation of the KPP–Fisher equation.

In the present work, we are concerned with determining the propagation speeds of premixed combustion and invasion waves as simulated by the stochastic model with competitive mixing and finite correlation time of particle motions. We examine the statistically-stationary state in which the propagation speed is constant, and the governing equations admit a steady solution (in a frame moving with the wave). The cases of very large and very small Damkohler numbers and different localisations of mixing are considered. We also investigate the effect of having a limited number of particles in the simulations. The results are validated by stochastic simulations.

In the next section we describe the particle system considered and the statistical equations which describe it. In Sections 3 and 4 solutions for the flame speed are obtained for the case in which mixing is localised only in physical space. Numerical simulations confirming and extending these results are given in Section 5. In Section 6 we consider the case in which mixing is localised in both physical and velocity spaces. The results obtained are discussed in the context of turbulent premixed flame propagation in Section 7. A solution for the problem of the propagation speed of disturbances carried by Brownian particles in one-dimensional space is presented separately in Appendix A.

## 2. Particle systems and governing equations

In the first three subsections we describe the particle system considered for: (1) the statistically-homogeneous case; (2) the one-dimensional case with diffusive motion; and

Table 1. Rules for competitive mixing.

The rule for mixing				
Before mixing		After mixing		Probability of event
$Y_p$	$Y_q$	$\dot{Y}_p$	$\dot{Y}_q$	
0	0	0	0	$(1 - \langle Y \rangle)^2$
0	1	1	1	$\langle Y \rangle (1 - \langle Y \rangle)$
1	0	1	1	$\langle Y \rangle (1 - \langle Y \rangle)$
1	1	1	1	$\langle Y \rangle^2$

(3) the one-dimensional case with finite correlation time of the particles' velocity. The latter case includes the other two as special cases, and its governing statistical equation is derived in the subsequent subsections.

### 2.1. The homogeneous case

We consider Pope particles with property  $Y$  and two-particle mixing defined according to the rules of competitive mixing. The rules for mixing a couple of particles, say particles  $p$  and  $q$ , are given in Table 1.

The last column indicates the probability of occurrence of the mixing event, not the probability of the outcome, which is certain. This rule is the most simple form of competitive mixing with only two particle states allowed:  $Y = 1$  representing winners and  $Y = 0$  representing losers. Assuming that all couples are formed with equivalent probability, the value of  $\langle Y \rangle$  represents the fraction of the winners among the particles, and the probabilities of each mixing event are given in the last column of the table (assuming stochastic independence of particles). Note that these probabilities sum to one and that only the second and third cases change particle values.

In a homogeneous case with a large number of particles, the rate of change of the mean  $\langle Y \rangle$  is given by the following equation:

$$\frac{d\langle Y \rangle}{dt} = 2\omega_m \langle Y \rangle (1 - \langle Y \rangle), \quad (1)$$

where  $\omega_m$  is the number of couples formed per unit time divided by the total number of particles, while  $2\langle Y \rangle(1 - \langle Y \rangle)$  is the probability of a change in particle values. For example, if all  $n_p$  particles form  $n_p/2$  couples within each time step  $\Delta t$ , then  $\omega_m = (2\Delta t)^{-1}$ .

The mixing scheme considered here corresponds to a number of physical processes in inhomogeneous systems: invasion of a strong competitor into a domain occupied by weaker participants, or premixed combustion with very fast reaction rates. In the latter case, any disturbance of the initial unburned state  $Y = 0$  leads to intensive combustion and rapid change of  $Y$  to its final burned state of  $Y = 1$ . The BML theory of turbulent premixed combustion indicates a source-term structure similar to Equation (1).

### 2.2. Inhomogeneous diffusive case: the KPP-Fisher Equation

If the particles are uniformly distributed in physical space and move in physical space according to the following stochastic differential equation:

$$dx^* = (2\mathcal{D}_0)^{1/2} dw, \quad (2)$$

where  $w(t)$  denotes a Wiener process, then the value  $\langle Y \rangle$  satisfies the KPP–Fisher Equation [21, 22]

$$\frac{\partial \langle Y \rangle}{\partial t} - \mathfrak{D}_0 \frac{\partial^2 \langle Y \rangle}{\partial x^2} = 2\omega_m \langle Y \rangle (1 - \langle Y \rangle) \tag{3}$$

Equation (3) differs from Equation (1) by the diffusional term in (3) that appear due to inhomogeneous effects. It should be noted that independence of particles is assumed in evaluation of probabilities of forming different couples – these probabilities are shown in Table 1. As considered by Klimenko [26] for conservative mixing, dependencies between particles result in a reduction of the effective mixing rate.

The theory for Equation (3), which was developed by KPP, indicates that, although Equation (3) allows for steady waves  $\partial \langle Y \rangle / \partial t = -s \partial \langle Y \rangle / \partial x$  propagating with the speed  $s$  that may take different values

$$s \geq s_{\min} = 2\sqrt{2\omega_m \mathfrak{D}_0}, \tag{4}$$

it is the speed  $s_{\min}$ , however, that is realizable in most practical cases when the gradients of the initial conditions have a finite support (and this is the case in computer simulations and experiments). In the rest of the paper we use  $s_{\min}$  by default as the wave speed for KPP-type equations. It can be noted that the representation considered here is an alternative stochastic representation for a ‘simple epidemic process’ or a ‘simple invasion’ which was studied by Fisher, KPP and many others [23, 25]. The stochastic representations of KPP-type equations are, of course, not limited to the stochastic model based on competitive mixing and presented here. For example, the KPP–Fisher source term can be recovered by simply setting the probability of conversion of the particle values from  $Y = 0$  to  $Y = 1$  to be proportional to  $\langle Y \rangle$  [27].

### 2.3. Particle motion with finite velocity correlation time

Consider the system of stochastic differential equations

$$dx^* = u^* dt, \tag{5}$$

$$du^* = -u^* \frac{dt}{\tau_*} + \left(2 \frac{u^{*2}}{\tau_*}\right)^{1/2} dw, \tag{6}$$

where the particle velocity  $u^*$  is modelled by the Ornstein–Uhlenbeck (OU) process with mean  $\langle u^* \rangle = 0$ , variance  $\langle (u^*)^2 \rangle = u_*^2$  and the autocorrelation time scale  $\tau_*$ . These equations take into account that motions in physical space may have a finite correlation time  $\tau_*$ . For example, in turbulent premixed combustion, velocity changes have a characteristic correlation time determined by turbulence macro-scales.

With  $x$  and  $u$  being sample space variables corresponding to  $x^*$  and  $u^*$ , we define the joint PDF of  $x^*(t)$  and  $u^*(t)$  to be  $f(x, u, t)$ . This can be expressed as

$$f = \langle \psi \rangle, \quad \psi \equiv \delta(u^* - u) \delta(x^* - x), \tag{7}$$

where  $\psi$  is a fine-grained PDF. It follows from Equations (5) and (6) that  $f$  evolves by the Fokker–Planck equation

$$\frac{\partial f}{\partial t} + u \frac{\partial f}{\partial x} - \frac{1}{\tau_*} \left( \frac{\partial u f}{\partial u} + u_*^2 \frac{\partial^2 f}{\partial u^2} \right) = 0. \quad (8)$$

For the statistically-stationary case of interest, Equation (8) has a solution

$$f(x, u) = \frac{f_0(u)}{l_0}, \quad f_0(u) \equiv \frac{1}{\sqrt{2\pi u_*^2}} \exp\left(-\frac{u^2}{2u_*^2}\right), \quad (9)$$

where  $l_0$  represents the length of the domain under consideration.

#### 2.4. Length and times scales

We consider  $n_p$  particles uniformly spaced in the  $x$ -domain of length  $l_0$ . Thus the mean particle spacing  $l_p$  and the associated time scale are

$$l_p = l_0/n_p, \quad \tau_p = l_p/u_*. \quad (10)$$

Based on the parameters  $u_*$  and  $\tau_*$  defining the OU process, we can define the convective length scale

$$l_* = u_* \tau_*. \quad (11)$$

There are two independent non-dimensional parameters in the problem, which we take to be

$$D = 2 \frac{\tau_*}{\tau_m} \quad \text{and} \quad R = \frac{\tau_*^2}{\tau_p^2} = \frac{l_*^2}{l_p^2}, \quad (12)$$

where  $\tau_m \equiv 1/\omega_m$ . As the parameters  $D$  and  $R$  resemble the Damkohler and Reynolds numbers, they can be referred to as modelling Damkohler and Reynolds numbers or, when this cannot cause confusion, simply as Damkohler and Reynolds numbers. It should be noted, however, that these parameters do not coincide with the physical Damkohler and Reynolds numbers used in the last section.

Another relevant time scale is the ‘collision time scale’  $\tau_c$  defined as the time for the r.m.s. particle displacement to reach the interparticle spacing difference  $l_p$ . Thus,  $\tau_c$  is a measure of the time between a particle acquiring new partners. After time  $t$ , the variance of particle displacement is [7]

$$l_t^2(t) = 2u_*^2 \tau_* \left\{ t - \tau_* \left[ 1 - \exp\left(-\frac{t}{\tau_*}\right) \right] \right\}.$$

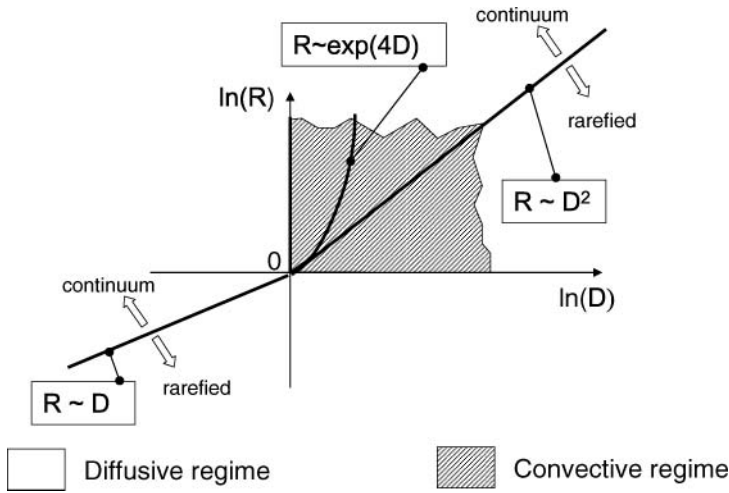


Figure 1. Regime diagram.

Thus  $\tau_c$  is such that  $l_t(\tau_c) = l_p$ . We can readily deduce the limiting behaviour

$$\tau_c = \frac{1}{2} \frac{\tau_p^2}{\tau_*}, \quad R \ll 1 \tag{13}$$

$$\tau_c = \tau_p, \quad R \gg 1. \tag{14}$$

In the case  $\tau_m \ll \tau_c$ , a particle will mix repeatedly with the same partner (approximately  $\tau_m/\tau_c$  times) before it acquires a new partner. Second and subsequent mixing with the same partner has no effect. Consequently, we define the ‘effective’ mixing time scale by

$$\tau_e = \max(\tau_m, \tau_c). \tag{15}$$

In the case  $\tau_c > \tau_m$  mixing is limited not by  $\omega_m$ , but by the rate of encountering new partners: we refer to this case as ‘rarefied’. The case  $\tau_c < \tau_m$  is referred to as ‘continuum’. If  $\tau_e$  is less than  $\tau_*$ , then the particle motion between non-trivial mixing events is ‘convective’ whereas if  $\tau_e$  is greater than  $\tau_*$  it is ‘diffusive’. The regime diagram is shown in Figure 1 (where the symbol ‘0’ indicates the coordinate origin  $\ln(D) = 0$  and  $\ln(R) = 0$ ), while major regimes are summarised in Appendix B.

In addition to the parameters  $D$  and  $R$ , we introduce the modelling Knudsen number  $K$ , which, when convenient, can be used in place of the modelling Reynolds number as the second non-dimensional parameter. This is defined by

$$K \equiv \frac{l_p}{l_m} = \left[ \frac{D(1+D)}{4R} \right]^{1/2} \approx \left\{ \begin{array}{ll} \left[ \frac{D}{4R} \right]^{1/2}, & D \ll 1 \\ \frac{D}{[4R]^{1/2}}, & D \gg 1 \end{array} \right\}, \tag{16}$$



where  $l_m$  is an approximation to the r.m.s. distance travelled by a particle in the time  $\tau_m$ , and is defined by

$$l_m^2 \equiv \frac{u_*^2 \tau_m^2}{1 + \frac{\tau_m}{2\tau_*}} = u_*^2 \tau_m^2 \frac{D}{1 + D}. \quad (17)$$

Note that for large modelling Damkohler number there is convective motion over time  $\tau_m$ , and Equation (17) yields  $l_m \approx u_* \tau_m$ , whereas for small modelling Damkohler number there is diffusive motion with  $l_m \approx \sqrt{2u_*^2 \tau_* \tau_m}$ . The significance of the Knudsen number is that  $K \ll 1$  and  $K \gg 1$  correspond to the continuum and rarefied regimes, respectively.

## 2.5. Transport equations

We now consider Pope particles with property  $Y = (0, 1)$  and binary mixing operation defined in Table 1. This model is very similar to the model of turbulent premixed combustion introduced by Pope and Anand [1] who have shown that, when the reactions are fast and reach the flamelet regime, the PDF of the progress variable  $Y$  is dominated by two states  $Y = 0$  (unburned) and  $Y = 1$  (burned) and mixing is predominantly controlled by mixing of these states. The probability of  $Y > \varepsilon$  and  $Y < 1 - \varepsilon$  where  $\varepsilon$  is any small value, is small and, in this region, the rate of change of the progress variable is controlled by  $dY/dt = \Phi(Y)$ . The function  $\Phi(Y)$  is determined by the laminar premixed solution and  $\Phi(Y)$  does not coincide with the chemical source term, although the function  $\Phi(Y)$  scaled in the same way as the chemical source term, that is  $\Phi \sim 1/\tau_r$  where  $\tau_r$  is the characteristic time of chemical reactions. The function  $\Phi(Y)$  is essentially positive for  $\varepsilon < Y < 1 - \varepsilon$  (while the chemical source term can be zero for a large section of this interval) and results in prompt evolution of  $Y$  from any positive value to the burned state of  $Y = 1$ . The exact shape of the function  $\Phi(Y)$  is not important – competitive mixing can be interpreted as a superposition of conventional Curl's mixing and the following very fast process of evolution into the burned state. Competitive mixing introduces an upper limit for the propagation speed of the flames simulated by the same particle scheme but with conventional mixing (i.e. Curl's model with the same intensity of mixing) combined with a finite rate chemistry. The degree of similarity of competitive mixing and conventional mixing schemes with fast chemistry depends on specific features of mixing and chemical kinetics. Competitive mixing matches the expected shape of the source term  $\Phi(Y)$ , which was investigated in [1], reasonably well.

In the laminar case, the function  $\Phi(Y)$  and time  $\tau_r$  determine the overall flame propagation rate. However, in turbulent flows the rate of mixing between two dominant states of  $Y = 0$  and  $Y = 1$  determines the intensity of the combustion processes and the overall propagation speed. Note that the characteristic time of mixing  $\tau_m = \omega_m^{-1}$  may depend on, but is not necessarily equal to, the characteristic reaction time  $\tau_r$ . As discussed by Pope and Anand [1], this analysis is valid only for the flamelet regime. If only the reaction zone remains thin compared to the smallest scales in turbulence (thin reaction zone regime), no function  $\Phi(Y)$  can be deduced and, after mixing, evolution is controlled by the chemical source term  $W(Y)$ , which, typically, is essentially positive only for  $1 - \varepsilon_r < Y < 1$  where  $\varepsilon_r$  is usually small. In this case, complete conservative mixing of the burned  $Y = 1$  and unburned  $Y = 0$  states results in two particles with  $Y = 1/2$ . If the reaction zone is thin, these values are still away from the reaction zone and do not evolve to the burned state

even if the reactions are very fast at  $1 - \varepsilon_r < Y < 1$ . In the present work we, however, investigate the properties of the model for the whole range of the model parameters.

We define

$$h = \langle Y\psi \rangle, \quad g = \langle (1 - Y)\psi \rangle, \tag{18}$$

so that, obviously

$$h + g = f. \tag{19}$$

The equation for  $g$  can be derived from (5) and (6) by the standard technique using the Delta-functions [28]

$$\frac{\partial g}{\partial t} + u \frac{\partial g}{\partial x} - \frac{1}{\tau_*} \left( \frac{\partial u g}{\partial u} + u_*^2 \frac{\partial^2 g}{\partial u^2} \right) = - \left\langle \frac{dY}{dt} \psi \right\rangle. \tag{20}$$

The primary quantity we will examine is  $\hat{g}(x, u)$  defined as

$$\hat{g}(x, u) = \frac{g(x, u)}{f(u)} = \frac{\langle (1 - Y)\psi \rangle}{\langle \psi \rangle} = \langle (1 - Y) | x, u \rangle, \tag{21}$$

where the condition in the last conditional term is used as an abbreviation for  $x^* = x$  and  $u^* = u$ . Similarly we define

$$\hat{h}(x, u) = \frac{h(x, u)}{f(u)} = \langle Y | x, u \rangle, \tag{22}$$

and clearly we have

$$\hat{g}(x, u) + \hat{h}(x, u) = 1. \tag{23}$$

From Equations (8) and (20) we obtain

$$\frac{\partial \hat{g}}{\partial t} + u \frac{\partial \hat{g}}{\partial x} + \frac{1}{\tau_*} \left( u \frac{\partial \hat{g}}{\partial u} - u_*^2 \frac{\partial^2 \hat{g}}{\partial u^2} \right) = W \equiv - \frac{1}{f} \left\langle \frac{dY}{dt} \psi \right\rangle = - \left\langle \frac{\partial Y}{\partial t} \middle| x, u \right\rangle. \tag{24}$$

Expressions for  $W$  are derived in the following subsections.

**2.6. Dimensionless form of the transport equations**

The dimensionless form of Equations (24) is given by

$$\frac{\partial \hat{g}}{\partial T} + U \frac{\partial \hat{g}}{\partial X} + \frac{1}{D_e} \left( U \frac{\partial \hat{g}}{\partial U} - \frac{\partial^2 \hat{g}}{\partial U^2} \right) = \tilde{W}, \tag{25}$$

where

$$\tilde{W} \equiv \frac{W}{2\omega_e} = -\frac{1}{2\omega_e f} \left\langle \frac{\partial Y}{\partial t} \psi \right\rangle = -\frac{1}{2\omega_e} \left\langle \frac{\partial Y}{\partial t} \middle| x, u \right\rangle, \quad (26)$$

$$T = 2\omega_e t, \quad X = 2\frac{\omega_e}{u_*} x, \quad U = \frac{u}{u_*}, \quad D_e = 2\omega_e \tau_*, \quad (27)$$

the value of  $\omega_e = 1/\tau_e$  represents the effective mixing frequency and the effective number  $D_e$  indicates the relative intensity of the source term. Equations (12)–(14) indicate that

$$D_e = \begin{cases} D, & \tau_c \ll \tau_m \\ 4R, & \tau_c \gg \tau_m, \quad R \ll 1 \\ 2R^{1/2}, & \tau_c \gg \tau_m, \quad R \gg 1. \end{cases} \quad (28)$$

The distribution  $f_0$  defined by (9) satisfies the following dimensionless equation:

$$\frac{dU f_0}{dU} + \frac{d^2 f_0}{dU^2} = 0. \quad (29)$$

A mixing event can result in a change in particle values only if the mixing couple is formed between new particles while repeated mixing does not change particle values for the competitive mixing scheme considered here. Thus, the effective mixing frequency  $\omega_e \approx \min(\omega_m, \omega_c)$  can be estimated as the minimum of two values: the mixing frequency  $\omega_m$  and the collision frequency  $\omega_c$ . Since  $\omega_c = \omega_c(U)$  can vary over the domain, this definition needs some clarification: the propagation speed is determined as the minimum of the flame speeds determined with  $\omega_e = \omega_m$  and  $\omega_e = \omega_c$ . Assuming that each particle forms a couple with its closest neighbour, collision is understood here as a neighbour change. Neighbourhood can be defined by the distance  $x$  in physical space or in  $u$ - $x$  phase space. This change is determined by the number of particles and the intensity of their random walk. In the rarefied case,  $\omega_c$  determines the rate of change of  $\langle Y \rangle$  while if the particles are densely distributed then  $\omega_m$  is the determining parameter. We note that the mixing frequency is an input parameter of the system, whose exact value is known, while the collision frequency depends on the other conditions of the simulations and can be estimated rather than specified exactly. Thus, effective replacement of  $\omega_m$  by  $\omega_c$  in rarefied flows is approximate and can be used only for estimations.

### 2.7. Steadily propagating wave

In most cases, we are interested in long-time asymptotics when a wave with the steadily propagating speed is formed. The steady-state version of Equation (25) is given by

$$(U - S) \frac{\partial \hat{g}}{\partial Z} + \frac{1}{D_e} \left( U \frac{\partial \hat{g}}{\partial U} - \frac{\partial^2 \hat{g}}{\partial U^2} \right) = \tilde{W}, \quad (30)$$

where  $S = s/u_*$  is the non-dimensional wave speed, and  $Z = (X - ST)$  is the dimensionless coordinate attached to the front. The boundary conditions for steady propagation of a

wave are given by the relations

$$\hat{g} \rightarrow 0 \text{ as } Z \rightarrow -\infty \tag{31}$$

in the burned state and

$$\hat{g} \rightarrow 1 \text{ as } Z \rightarrow +\infty \tag{32}$$

in the unburned state.

**2.8. Localisation of mixing in the physical space**

A precise description of the mixing process is as follows. Given the ensemble of  $n_p$  particles, ‘primary’ particles are selected (randomly with equal probability) at the rate  $n_p \omega_m$ . For each primary particle a ‘secondary’ is selected: in the present case the secondary particle is the primary particle’s nearest neighbour in physical space.

The quantity  $W$  in Equation (24) has, for notational convenience, been written as  $W = \langle dY/dt|x, u \rangle$ . However because  $Y$  changes discontinuously it is more precisely defined as

$$W(x, u, t) = \lim_{\Delta t \rightarrow 0} \left( \frac{1}{\Delta t} \langle \Delta Y|x, u \rangle \right), \tag{33}$$

where  $\Delta Y = Y(t + \Delta t) - Y(t)$  is defined as the increment. Although  $Y$  changes discontinuously from 0 to 1, the averages of  $Y$  typically display a more continuous behaviour as indicated by KKP-type source terms in the average equations considered in Section 2.2 and below. Let us consider particle  $Y^{(q)}$ . In a small time interval  $\Delta t$  it has probability  $\omega_m \Delta t$  of being selected as a primary particle, in which case we denote its secondary particle as  $Y^{(s)}$  (the compositions of the primary and secondary particles are denoted by  $Y^{(p)}$  and  $Y^{(s)}$ ). Particle  $Y^{(q)}$  also has probability  $\omega_m \Delta t$  of being selected as a secondary particle of a selected primary particle,  $Y^{(p)}$ . Then we have:  $\Delta Y^{(p)} = 1$  if  $Y^{(p)}(t) = 0$ ,  $Y^{(s)}(t) = 1$ ; otherwise  $\Delta Y^{(p)} = 0$ . Similar relations are valid for  $\Delta Y^{(s)}$ . These considerations lead to the result

$$\begin{aligned} W(x, u, t) &= \lim_{\Delta t \rightarrow 0} \left( \frac{1}{\Delta t} \langle \Delta Y^{(q)}|x, u \rangle \right) \\ &= -\omega_m \text{Prob} \{ Y^{(q)}(t) = 0, \quad Y^{(s)}(t) = 1 | x^{(q)} = x, \quad u^{(q)} = u \} \\ &\quad -\omega_m \text{Prob} \{ Y^{(q)}(t) = 0, \quad Y^{(p)}(t) = 1 | x^{(q)} = x, \quad u^{(q)} = u \}. \end{aligned} \tag{34}$$

Now the two particles  $Y^{(p)}$  and  $Y^{(s)}$  are statistically identical (but not necessarily statistically independent). And so we have

$$\begin{aligned} W(x, u, t) &= -2\omega_m \text{Prob} \{ Y = 0, \quad Y^{(s)} = 1 | x, u \} \\ &= -2\omega_m \text{Prob} \{ Y^{(s)} = 1 | x, u, \quad Y = 0 \} \langle (1 - Y)|x, u \rangle. \end{aligned} \tag{35}$$

For the case of localisation in physical space only, the selection of the secondary particle does not depend on the primary particle velocity and

$$W(x, u, t) = -2\omega_m \text{Prob} \{Y^{(s)} = 1|x, Y = 0\} \langle (1 - Y)|x, u \rangle. \quad (36)$$

For the continuum case, the probability of two particles pairing with each other repeatedly is very small, and so independence can be assumed. Thus for localisation in physical space in the continuum regime we have

$$W = -2\omega_m \langle Y|x \rangle \langle (1 - Y)|x, u \rangle = -2\omega_m \bar{h} \hat{g}. \quad (37)$$

Here, we introduce the averages

$$\begin{aligned} \bar{h}(x) &= \langle Y|x \rangle = \int_{-\infty}^{+\infty} \hat{h} f_0 \, du, \\ \bar{g}(x) &= \langle (1 - Y)|x \rangle = \int_{-\infty}^{+\infty} \hat{g} f_0 \, du. \end{aligned}$$

It is clear that

$$\bar{h}(x) + \bar{g}(x) = \int_{-\infty}^{+\infty} f_0(x, u) \, du = 1. \quad (38)$$

For the rarefied case, the two particles repeatedly mix with each other (with no effect after the first mixing) and so independence certainly cannot be assumed. It is more reasonable to assume independence for mixing with a new partner, which occurs at the rate  $\omega_c$ . Hence, in the rarefied case, the approximation is

$$W = -2\omega_c \bar{h} \hat{g}. \quad (39)$$

For the normalised source  $\tilde{W} = W/(2\omega_c)$ , the above two equations can be written in the common form

$$\tilde{W} = -\Omega \bar{h} \hat{g}, \quad (40)$$

where  $\Omega \approx 1$  is the ratio between the effective mixing rate and its estimate  $\omega_c$ .

The formulae determining  $\tau_c$  for localisation of mixing in physical space were specified previously by (13) and (14).

## 2.9. Localisation of mixing in the phase space

We now consider the case in which mixing is localised in the  $x$ - $u$  phase space. It is most conventional to consider the non-dimensional phase space of  $\tilde{x} = x/l_*$  and  $U = u/u_*$ . We also introduce non-dimensional time  $\tilde{t} = t/\tau_*$ . Mixing is performed by selecting a primary particle as previously but now the secondary particle is selected to be the primary particle's nearest neighbour in  $\tilde{x}$ - $U$  space.

The analysis for  $W$  proceeds as in the previous subsection but now the conditioning on  $u$  is needed which leads to the result

$$\tilde{W} = -\Omega \hat{h} \hat{g}, \tag{41}$$

i.e.  $\hat{h} = \langle Y|x, u \rangle$  in place of  $\bar{h} = \langle Y|x \rangle$ .

We now determine collision frequencies for localisation of mixing in the phase space. First we note that in the rarefied case  $\tau_* \ll \tau_p$  a particle quickly ‘forgets’ its initial location in the velocity space and conditioning of mixing on  $u$  does not have any effect. Hence we still use Equation (13), although Equation (14) needs corrections to be applicable to mixing with phase-space localisation as considered below.

In  $\tilde{x}$ - $U$  space, the particle number density is

$$\tilde{n} = n_p f u_*^2 \tau_* = \frac{1}{\sqrt{2\pi}} \frac{l_*}{l_p} \exp\left(-\frac{U^2}{2}\right), \tag{42}$$

where Equation (9) has been used for  $f$ . The mean square nearest neighbour distance  $\tilde{d}^2$  is the inverse of  $\tilde{n}$  :

$$\tilde{d}^2 = \sqrt{2\pi} \frac{l_p}{l_*} \exp\left(\frac{U^2}{2}\right). \tag{43}$$

Note that this distance depends on  $U$  and increases with  $|U|$ .

Consider two particles labelled ‘p’ and ‘s’ initially with the same position and velocity, both evolving according to Equations (5)–(6) (with independent Wiener processes). An analysis based on Equations (5)–(6) shows that the mean square separation of the particles in  $\tilde{x}$ - $U$  space is

$$\begin{aligned} \tilde{r}^2(\tilde{t}) &\equiv \left\langle (\tilde{x}^{(p)}(t) - \tilde{x}^{(s)}(t))^2 \right\rangle + \left\langle (U^{(p)}(t) - U^{(s)}(t))^2 \right\rangle \\ &= 4 \left( \tilde{t} - 1 + e^{-\tilde{t}} \right) + 2 \left( 1 - e^{-2\tilde{t}} \right) \approx 4\tilde{t}. \end{aligned} \tag{44}$$

In the second line, the first term is the dispersion in  $\tilde{x}$ , which dominates for  $\tilde{t} > 1$ , and the second term is the dispersion in  $U$ , which dominates for  $\tilde{t} < 1$ . Interestingly, the approximation  $\tilde{r}^2 \approx 4\tilde{t}$  is valid for both very short and very long times while being applicable with 10% accuracy to all  $\tilde{t}$ .

For short times when  $\tau_c \ll \tau_*$  we determine the collision time  $\tau_c$  from the condition  $\tilde{r}(\tau_c/\tau_*) = \tilde{d}$ , i.e.

$$\tau_c = \tau_{c0} \exp\left(\frac{1}{2} \frac{u^2}{u_*^2}\right), \quad R \gg 1, \tag{45}$$

where

$$\tau_{c0} = \sqrt{\frac{\pi}{8}} \tau_p \approx \tau_p \tag{46}$$

is the centreline value of  $\tau_c$ . Equations (45) and (46) replace (14) when conditioning of mixing is performed on both  $x$  and  $u$ .

### 3. Diffusive regime $D_e \ll 1$

In this section, we analyse the diffusive regime  $D_e \ll 1$ . Since we use the effective mixing frequency, the analysis is applicable both to the continuum regime and, approximately, to the rarefied regime. These results are also applicable to both the physical-space and phase-space localisations, as particles ‘forget’ their initial positions in the velocity space between mixing events. Consider Equation (25)

$$\frac{\partial \hat{g}}{\partial T} + \frac{U}{D_e^{1/2}} \frac{\partial \hat{g}}{\partial \tilde{X}} + \frac{1}{D_e} \left( U \frac{\partial \hat{g}}{\partial U} - \frac{\partial^2 \hat{g}}{\partial U^2} \right) = \tilde{W} \quad (47)$$

at the limit of  $D_e \rightarrow 0$ , which corresponds to the diffusive regime. Here, we introduce characteristic coordinate  $\tilde{X} = X/D_e^{1/2}$ . The source term is given either by Equation (40) for the physical-space localisation or by Equation (41) for the phase-space localisation of mixing. Expanding  $\hat{g}$  into the series

$$\hat{g} = \hat{g}_0 + D_e^{1/2} \hat{g}_1 + D_e \hat{g}_2 + \dots \quad (48)$$

results in

$$U \frac{\partial \hat{g}_0}{\partial U} - \frac{\partial^2 \hat{g}_0}{\partial U^2} = 0 \quad (49)$$

$$U \frac{\partial \hat{g}_1}{\partial U} - \frac{\partial^2 \hat{g}_1}{\partial U^2} = -U \frac{\partial \hat{g}_0}{\partial \tilde{X}} \quad (50)$$

$$U \frac{\partial \hat{g}_2}{\partial U} - \frac{\partial^2 \hat{g}_2}{\partial U^2} = -\frac{\partial \hat{g}_0}{\partial T} - U \frac{\partial \hat{g}_1}{\partial \tilde{X}} + \tilde{W}_0, \quad (51)$$

where  $\tilde{W}_0 = \tilde{W}(\hat{g}_0)$  does not depend on  $U$ . Integration of these equations yields

$$\hat{g}_0 = \hat{g}_0(T, \tilde{X}), \quad \hat{g}_1 = -U \frac{\partial \hat{g}_0}{\partial \tilde{X}} \quad (52)$$

and

$$U \frac{\partial \hat{g}_2}{\partial U} - \frac{\partial^2 \hat{g}_2}{\partial U^2} = -\frac{\partial \hat{g}_0}{\partial T} + U^2 \frac{\partial^2 \hat{g}_0}{\partial \tilde{X}^2} + \tilde{W}_0. \quad (53)$$

Multiplication of this equation by  $f_0(U)$  and integration over all  $U$  (while taking Equation 29 into account) indicates that

$$\frac{\partial \hat{g}_0}{\partial T} = \frac{\partial^2 \hat{g}_0}{\partial \tilde{X}^2} + \tilde{W}_0, \quad (54)$$

where we use that

$$\int_{-\infty}^{+\infty} U^2 f_0 dU = 1,$$

or, in the dimensional form this equation,

$$\frac{\partial \hat{g}_0}{\partial t} = \mathfrak{D}_\tau \frac{\partial^2 \hat{g}_0}{\partial x^2} + W_0, \quad \mathfrak{D}_\tau \equiv u_*^2 \tau_*, \tag{55}$$

is essentially identical to the KPP–Fisher Equation (3). We note that at the leading order the expression for the source term is the same for physical-space (40) and phase-space (41) localisations  $\tilde{W}_0 = -(1 - \hat{g}_0)\hat{g}_0$  since  $\hat{g}_0$  does not depend on  $U$  and we put  $\Omega = 1$  here. The equation for the minimal flame speed takes the form

$$s = u_* S = 2\sqrt{2\mathfrak{D}_\tau \omega_c} = 2u_* D_e^{1/2}, \quad D_e = 2\omega_c \tau_*. \tag{56}$$

This equation is derived for both the continuous regime where  $S = 2D^{1/2}$  and for the rarefied regime but for the rarefied regime this equation becomes an estimate of  $S \approx 4R^{1/2}$  according to (28). With the use of Equation (13) to estimate  $\tau_c$ , the speed  $s$  becomes for the rarefied case

$$s = C_0 u_* \frac{\tau_*}{\tau_p} = C_0 \frac{u_*^2 \tau_*}{l_p} = C_0 \frac{\mathfrak{D}_\tau}{l_p}, \tag{57}$$

where the constant  $C_0$  depends on the detail of the mixing process. This constant is determined in Appendix A for the special case of Brownian relay, where particles mix instantaneously when their trajectories in  $x$ -space intersect.

In the continuum regime the thickness of the flame is determined by the condition  $\Delta \tilde{X} \sim 1$ ,  $\Delta X \sim D^{1/2}$  or  $\Delta x \sim u_*(\tau_*/\omega_m)^{1/2}$  or  $\Delta \tilde{x} \equiv \Delta x/l_* \sim D^{-1/2}$ , while in the rarefied case the flame location is an imaginary line separating particles with  $Y = 1$  on one side from particles with  $Y = 0$  on the other side.

The steady wave version of Equation (47) is given by

$$\frac{U - S}{D_e^{1/2}} \frac{\partial \hat{g}}{\partial \tilde{Z}} + \frac{1}{D_e} \left( U \frac{\partial \hat{g}}{\partial U} - \frac{\partial^2 \hat{g}}{\partial U^2} \right) = \tilde{W}, \tag{58}$$

where  $\tilde{Z} = \tilde{X} - ST/D_e^{1/2}$ . This equation after multiplication by  $f_0$  and taking into account (29) can be transformed into

$$\frac{\partial}{\partial \tilde{Z}} \left( \frac{U - S}{D_e^{1/2}} \hat{g} f_0 \right) + \frac{1}{D_e} \frac{\partial}{\partial U} \left( U \hat{g} f_0 - \frac{\partial \hat{g}}{\partial U} f_0 \right) = \tilde{W} f_0.$$

Integration of this equation over all  $U$  and  $\tilde{Z}$ , while taking into account Equation (9) and also that  $\hat{g} \rightarrow 1$  as  $\tilde{Z} \rightarrow +\infty$  and  $\hat{g} \rightarrow 0$  as  $\tilde{Z} \rightarrow -\infty$ , yields

$$\frac{S}{D_e^{1/2}} = - \int_{-\infty}^{+\infty} \int_{-\infty}^{+\infty} \tilde{W} f_0 dU d\tilde{Z}. \tag{59}$$



Substitution of the asymptotic series  $\tilde{W} = \tilde{W}_0 + D_e^{1/2}\tilde{W}_1 + D_e\tilde{W}_2 + \dots$ , where the terms are determined by the series (48) and Equations (40) or (41), results in

$$\frac{S}{D_e^{1/2}} = S_0 + D_e S_2 + \dots \quad (60)$$

The term  $S_1$  is not present for both cases (40) and (41) since  $\hat{g}_1$  is an odd function of  $U$ , i.e.  $\hat{g}_1(-U) = -\hat{g}_1(U)$ . The value of  $S_0 = 2$  is determined from Equation (56), while finding  $S_2$  needs numerical integration for the wave solution of the KPP–Fisher equation and can be different for the source terms defined by (40) and (41).

#### 4. The convective regime $D_e \gg 1$ with physical-space localisation of mixing

The convective regime  $D_e \gg 1$  is considered in this section for the case of localisation of mixing in the  $x$ -space. Both continuum and rarefied regimes are analysed. The transport Equation (30) for this case takes the form

$$(U - S) \frac{\partial \hat{g}}{\partial Z} + \frac{1}{D_e} \left( U \frac{\partial \hat{g}}{\partial U} - \frac{\partial^2 \hat{g}}{\partial U^2} \right) = -\Omega \bar{h} \hat{g}. \quad (61)$$

Here we note that the particle density in physical space is constant since as discussed previously  $f = f_0(U)/l_0$  and thus we expect that  $\omega_e = \text{const}$  and  $\Omega = 1$ .

##### 4.1. The major transformation zone

The regular expansion

$$\hat{g} = \hat{g}_0 + \frac{\hat{g}_1}{D_e} + \dots,$$

substituted into Equation (61) results in

$$(U - S) \frac{\partial \hat{g}_0}{\partial Z} = -\bar{h}_0 \hat{g}_0, \quad (62)$$

which can be integrated while taking into account unburned boundary conditions for  $U < S$  and burned boundary conditions for  $U > S$  resulting in

$$\begin{aligned} \text{(a) } \hat{g}_0 &= 1, & Z &\geq Z_0 \\ \text{(b) } \hat{g}_0 &= \exp\left(\frac{-1}{S-U} \int_Z^{Z_0} \bar{h}_0 dZ\right), & Z &\leq Z_0, \quad U < S \\ \text{(c) } \hat{g}_0 &= 0, & U &\geq S, \end{aligned} \quad (63)$$

where

$$\bar{h}_0(Z) = \int_{-\infty}^{\infty} (1 - \hat{g}_0) f_0(U) dU = 1 - \int_{-\infty}^{\infty} \hat{g}_0 f_0(U) dU.$$

The line of  $U = S$  formally requires that either  $\hat{g}_0 = 0$  or  $\bar{h}_0 = 0$  (and  $\hat{g}_0 = 1$ ). This indicates the need for consideration of leading points located at  $U \geq S$  and  $Z \gtrsim Z_0$ , this analysis presented in the next subsection indicates that  $S$  is logarithmically larger than 1. Hence, we can approximately evaluate the integral for  $\bar{h}_0$  as

$$\bar{h}_0(Z) = 1 - \int_{-\infty}^{\infty} \hat{g}_0(Z, U) f_0(U) dU = 1 - \hat{g}(Z, 0) + O\left(\frac{U^2}{S^2}\right),$$

since  $\hat{g}_0$  can be expanded into the series

$$\hat{g}_0(Z, U) = \hat{g}(Z, 0) \left(1 + \frac{U}{S} + \frac{U^2}{S^2} + \dots\right),$$

obtained by expanding  $1/(S - U)$  and the exponent in (63b) into the power series of  $U/S$ . Substitution of  $\hat{g}(Z, 0) = 1 - \bar{h}_0(Z)$  into (63b) results in

$$\bar{h}_0(Z) = 1 - \exp\left(-\frac{1}{S} \int_Z^{Z_0} \bar{h}_0 dZ\right), \quad Z \leq Z_0.$$

Differentiating this equation indicates that we can write at the leading order

$$S \frac{\partial \bar{h}_0}{\partial Z} = -(1 - \bar{h}_0) \bar{h}_0. \tag{64}$$

The length of the transition zone where  $\bar{h}_0$  changes from 0 to 1 is determined, according to Equation (64), by  $\Delta Z \sim S$  or  $\Delta x \sim s/\omega_e \sim u_*/\omega_e$ .

**4.2. Maximal propagation speed**

The front speed cannot significantly exceed the speed  $u_{\max}$  of the fastest particles moving in the same direction as the flame (assuming mixing is well localised) since  $u_{\max}$  limits the speed of propagation of any disturbances in the system. Assuming the continuum regime, the number of particles within the transition zone (having the width of  $\Delta x \sim s\tau_m$ ) is determined by  $N \sim \Delta x/l_p \sim s\tau_m/l_p$ . With the use of a rough estimate  $s \sim u_*$  we obtain  $N \sim l_m/l_p = 1/K$ . The particle velocities have the standard Gaussian distribution (9) with the c.d.f. (cumulative distribution function)

$$F\left(\frac{u}{u_*}\right) = \int_{-\infty}^u f_0(u) du = \frac{1}{2} \left[1 + \operatorname{erf}\left(\frac{1}{\sqrt{2}} \frac{u}{u_*}\right)\right]. \tag{65}$$

Since the particles' motions are independent, the probability that all  $N$  particle have velocities less than  $u$  is  $(F(u/u_*))^N$ . If  $u_{\max}$  is defined as the median value (that is the value having the c.d.f. of  $1/2$ ) then  $F(u_{\max}/u_*) = 1/2^{1/N}$  and the expression for  $u_{\max}$  becomes

$$s \approx u_{\max} = u_* F^{-1}\left(2^{-1/N}\right) = u_* F^{-1}\left(2^{-C_K K}\right), \tag{66}$$

where  $C_K$  is constant and  $F^{-1}$  is the inverse of the function  $F$ . This equation provides an estimate for maximal propagation speed of the front as  $D \rightarrow \infty$ .

Downloaded by [Cornell University] at 12:20 18 August 2012

In a rarefied regime, the propagation velocity becomes independent of  $\tau_m$ . Hence  $u_{\max}/u_*$  should depend on  $R$ , but not on  $K$  or  $D$ . According to (16),  $K \sim D/R^{1/2}$  in this case. Assuming that the number of particles  $N$  in the leading group that may have a leading particle with highest velocity is proportional to  $R^{1/2}$  we obtain  $N \approx C_R R^{1/2}$  and

$$s \approx u_{\max} \approx u_* F^{-1} \left( 2^{-C_R/R^{1/2}} \right), \tag{67}$$

where  $C_R$  is constant and the exact propagation speed is likely to be dependent on the details of mixing.

Numerical diffusion can be prominent in the rarefied regime and this needs special consideration. The effective numerical diffusion coefficient can be estimated as  $\mathfrak{D}_n \sim l_p^2/\tau_c$  [26], while dimensional considerations indicate that the flame speed associated with numerical diffusion can be estimated as  $s_n \sim (\mathfrak{D}_n/\tau_c)^{1/2}$ . Since according to (14)  $\tau_c = \tau_p$  in this case, the speed  $s_n$  is estimated as  $s_n \sim l_p/\tau_p = u_*$ . The exact form of this equation depends on the details of the mixing process. One can see that the numerical diffusion can contribute substantially but not dominantly to the flame speed  $s$ .

**4.3. Analysis of the leading points for the continuum regime**

In this section, we consider leading points located at  $U \gtrsim S$  and  $Z \gtrsim Z_0$  and determine the propagation speed which remains unknown in the previous subsection. The importance of leading points for the propagation speed of turbulent premixed flames was pointed out by Kuznetsov and Sabelnikov [16]. Characteristic variables for the leading point zone are given by

$$v = (U - S) S, \quad \zeta = (Z - Z_0) \frac{S^3}{D_e}, \tag{68}$$

so that (61) rewritten for  $\hat{h} = 1 - \hat{g}$  takes the form

$$v \frac{\partial \hat{h}}{\partial \zeta} + (1 + \dots) \frac{\partial \hat{h}}{\partial v} - \frac{\partial^2 \hat{h}}{\partial v^2} = \frac{D_e}{S^2} \bar{h} (1 - \hat{h}) = \frac{D}{S^2} \bar{h} + \dots, \tag{69}$$

where, in the source term,  $\hat{g} = 1 - \hat{h} \approx 1$  (we neglect  $\hat{h}$  as both  $\hat{h}$  and  $\bar{h}$  must be small in this zone). It is also expected that  $S$  is weakly large – that is  $S$  increases with increasing  $D$  but very slowly. Obtaining the solution for this equation may be quite difficult (instead we provide a numerical solution of the whole problem obtained by stochastic simulations) but our analysis needs only estimates that can balance the major terms in the equation.

Approximate evaluation of the integral for  $\bar{h}$

$$\bar{h} = \int_{-\infty}^{\infty} \hat{h} f_0 \, du = \int_0^{\infty} \frac{\hat{h}}{\sqrt{2\pi}} \exp \left[ - \left( \frac{S^2}{2} + v + \dots \right) \right] \frac{dv}{S} \sim \frac{\exp(-S^2/2)}{S} \hat{h} \tag{70}$$

indicates that

$$\frac{\exp(-S^2/2)}{S} \frac{D_e}{S^2} \sim \text{const}, \tag{71}$$

as the reaction term must be present at the leading order. If we neglect  $S$ , which only weakly depends on  $D_e$ ,

$$\exp\left(-\frac{S^2}{2}\right) D_e \sim \text{const} \quad \text{or} \quad S \sim \sqrt{C_1 + 2 \ln(D_e)}. \quad (72)$$

The leading order terms are given by  $S^2 \sim 2 \ln(D)$  for the continuum regime and, according to Equation (14), by  $S^2 \sim \ln(R)$  for the rarefied regime.

$$s \sim u_* \sqrt{C_1 + 2 \ln(2\omega_e \tau_*)}, \quad (73)$$

where  $C_1$  is a constant. The length of the leading zone is given by  $\Delta Z \sim D_e/S^3$  or  $\Delta x \sim u_* \tau_*/S^3 \sim u_* \tau_*$ , i.e. leading points stretch far ahead of the major transformation zone.

In the evaluation of the integral (70) we used the infinite limit assuming that the number of particles is infinitely large and  $K$  is infinitely small. If this is not the case the upper limit in this integral needs to be replaced by  $u_{\max}$ . This removes a part of the integral that can be assessed according to

$$\int_{u_{\max}}^{\infty} f_0 \, du = 1 - \left(\frac{1}{2}\right)^{C_K K} \approx \ln(2) C_K K.$$

Hence

$$\bar{h} = \int_{-\infty}^{u_{\max}} \hat{h} f_0 \, du = \left[ \frac{\exp(-S^2/2)}{S} - \ln(2) C_K K \right] \hat{h} \quad (74)$$

and

$$[\exp(-S^2/2) - C_K^\circ K] D \sim \text{const} \quad \text{or} \quad S \sim \sqrt{C_1 - 2 \ln(D_e^{-1} + C_K^\circ K)}, \quad (75)$$

where  $C_K^\circ = \ln(2) C_K$ . In the continuum regime  $D_e = D$ . If  $K$  is very small, we obtain Equation (73). However, the line  $C_K^\circ K \sim 1/D$  separates  $K$ -limited and  $D$ -limited regimes and, if  $C_K^\circ K \gg 1/D$ , we obtain  $S \sim \sqrt{C_1 - 2 \ln(K)}$  where  $C_1^\circ$  is a new constant. This equation is a more approximate version of Equation (66), where a simple exponential estimate is used for  $F$ . Equation (75) is formulated for continuum regime but takes into account the effects of having a limited number of particles. In the rarefied regime, both terms  $D_e^{-1}$  and  $K$  become, as previously noted, proportional to  $R^{-1/2}$  so that  $S^2 \sim \ln(R)$ .

### 5. Stochastic simulations for mixing with physical-space localisation

Stochastic simulations are performed over the range of the parameters  $D$  and  $R$  and the observed flame speeds and thicknesses are compared to theoretical estimates.

#### 5.1. Numerical method

The OU parameters  $u_*$  and  $\tau_*$  are arbitrarily set to unity. Then, given the values of  $D$  and  $R$ , all other parameters in the problem are determined (e.g.  $\omega_m, l_p, \tau_e, \dots$ ). Initially the number of particles is set to  $n_p = 64$ , and the initial domain considered in  $x$  is  $[-l_0/2, l_0/2]$ , with

$l_0 = n_p l_p$ . The particles are initialised: the position  $x^*$  is uniformly random in  $[-l_0/2, l_0/2]$ ; the velocity  $u^*$  is random, standardised Gaussian; and the particle composition is set to  $Y = 1$  for  $x < 0$  and to  $Y = 0$  for  $x \geq 0$ . If during the simulation a particle with  $Y = 1$  reaches the right boundary, or a particle with  $Y = 0$  reaches the left boundary, then the domain is deemed to be too narrow. The simulation is then re-started with both  $n_p$  and  $l_0$  doubled.

The only numerical parameter,  $C$ , in the simulation is used to control the time step  $\Delta t$  according to  $\Delta t = C\tau_c$ . The convergence of the scheme with  $C$  has been verified, and the relatively small value  $C = 0.05$  is used in the simulations reported below.

A time step consists of three sub-steps:  $x^*$  and  $u^*$  are advanced for time  $\Delta t/2$ ; mixing is performed for time  $\Delta t$ ; and then  $x^*$  and  $u^*$  are again advanced for time  $\Delta t/2$ .

The  $x^*-u^*$  advance is performed exactly. That is, given their values at the beginning of the step, their values at the end of the step have a known joint normal distribution. Hence their values at the end of the step are drawn from this distribution. At the end of each  $x^*-u^*$  sub-step, reflective boundary conditions are applied and the values of  $Y$  crossing the boundary are checked (and, if necessary, the simulation is re-started in a larger domain).

On the mixing sub-step, each particle is selected with probability  $\Delta p \equiv \min(\omega_m \Delta t, 1)$  as a primary particle. Note that, in rarefied cases,  $\omega_m \Delta t$  can exceed unity, in which case all particles are primary particles. Then, for each primary particle, the secondary particle is determined as the closest neighbouring particle (in  $x$ -space). (A refinement, which accelerates the temporal convergence, is that in the case  $\Delta p < 0.1$ , the secondary particles are instead selected from the ensemble of non-primary particles.) The pair of particles then mix: if both have  $Y = 0$  at the start of the step, then their composition does not change; otherwise they both have  $Y = 1$  at the end of the step.

On each time step, the centre,  $x_c$ , and the width,  $\Delta x$ , of the flame are determined as follows. The function  $q(x)$  is defined by

$$q(x) = l_p^2 \sum (1 - Y | x^* < x) \sum (Y | x^* \geq x), \quad (76)$$

where the sums are over all particles. This approximates the quantity

$$\bar{q}(x) = \int_{-\infty}^x (1 - \langle Y \rangle) dx \int_x^{\infty} \langle Y \rangle dx. \quad (77)$$

Note that  $q(x)$  is zero outside the flame (on both sides) and is positive within the flame. Thus we define the centre  $x_c$  to be the centroid, such that

$$\sum q(x^*)(x_c - x^*) = 0, \quad (78)$$

and the width  $\Delta x$  is defined by

$$\Delta x^3 = l_p \sum q(x^*), \quad (79)$$

which is an approximation to

$$\overline{\Delta x^3} = \int_{-\infty}^{\infty} \left( \int_{-\infty}^x (1 - \langle Y \rangle) dx' \int_x^{\infty} \langle Y \rangle dx' \right) dx. \quad (80)$$

The above methodology provides a stable way to extract  $x_c$  and  $\Delta x$  from the particles, and it requires neither binning nor smoothing.

At the end of the step, the solution domain is shifted so that  $x_c$  is at its centre, and particles are added and removed at the boundaries as needed. It should be noted that all treatments at the boundaries are exact (since the particle distribution there is known).

The simulation is run for a time  $T = 100\tau_e$ . The statistically stationary state is achieved well before  $t = T/2$ . Between  $t = T/2$  and  $t = T$ , extracted statistics are time averaged.

The flame speed,  $s$ , in the stationary period is extracted in two ways. The first value, denoted  $s_x$ , is obtained as the slope of the linear fit to  $x_c(t)$  over the stationary period. The second value, denoted  $s_Y$ , is the consumption speed obtained as the time-average of

$$l_p \sum \Delta Y / \Delta t \approx \int_{-\infty}^{\infty} W(x) dx, \tag{81}$$

where  $\Delta Y$  denotes the change in  $Y$  for the particle over the time step. It has been verified that the values of  $s_x$  and  $s_Y$  obtained from the simulations are extremely close to each other.

For each case considered,  $M$  statistically independent identical simulations are performed in order to reduce the statistical errors, and to estimate confidence intervals. The value of  $M$  is at least 4, and at most 200, or the number needed to reduce the confidence interval in  $s$  to 4% of its value (whichever is less).

### 5.2. Continuum diffusive regime

The continuum diffusive regime considered here corresponds to  $D \ll 1$ ,  $K \ll 1$ . We now present results on the flame speed  $s$  and the flame thickness  $\Delta x$  obtained from simulations in the continuum diffusive regime.

Figure 2 shows the appropriately scaled flame speed (i.e.  $S/\sqrt{D} = s/(u_*\sqrt{D})$ ) against  $D$  for a range of values of  $K$ . As may be seen, as  $D$  decreases, there is little dependence on  $D$  for  $D < 10^{-2}$ . There is, however, a more appreciable dependence on  $K$ , which is more clearly revealed in Figure 3. The picture is similar for the flame thickness shown in Figures 4 and 5. The normalised flame thickness is defined by  $\Delta \tilde{x} = \Delta x/l_*$  and is denoted by  $L$  in the figures (i.e.  $L \equiv \Delta \tilde{x}$ ). This is consistent with the equations of Section 3.

In the extreme continuum diffusive limit ( $D \rightarrow 0$ ,  $K \rightarrow 0$ ), we expect to recover the Fisher–KPP value of the flame speed  $S = 2\sqrt{D}$ . It is evident from Figure 3 that  $S/\sqrt{D}$  increases quite slowly as  $K$  decreases, and it is not clear that the limiting value of two is attained. To examine this matter more closely, in Figure 6 we plot  $(2 - S/\sqrt{D})$  against  $K$ . As may be seen, the results are consistent with the Fisher–KPP limit being approached slowly, as  $S \sim \sqrt{D}(2 - K^{1/4})$ . (Since the number of particles in the simulation varies inversely with  $K$ , simulations for small values of  $K$  are expensive.)

### 5.3. Rarefied diffusive regime

The rarefied diffusive regime is defined by  $D \ll 1$ ,  $K \gg 1$ . Assuming that the diffusivity  $D_*$  and the particle spacing  $l_p$  are the only relevant parameters, dimensional analysis then leads to the scalings  $S \sim \sqrt{D}/K \sim \sqrt{R}$  and  $L \equiv \Delta \tilde{x} \sim K/\sqrt{D} \sim 1/\sqrt{R}$  (see Section 3). As shown in Figures 7 and 8 these scalings are clearly confirmed by the simulations.

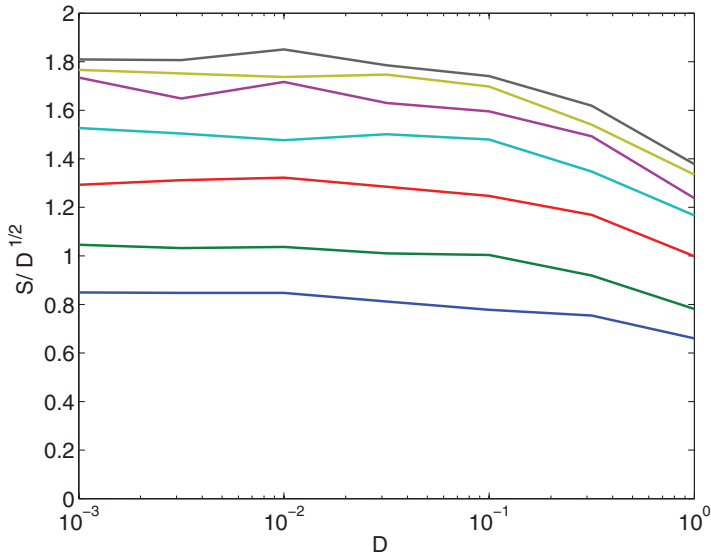


Figure 2. Scaled flame speed  $S/\sqrt{D}$  versus Damkohler number  $D$  in the continuum diffusive regime. The curves (from bottom to top) are for Knudsen number  $K = 10^{-k/2}$  for  $k = 0, 1, \dots, 6$ .

#### 5.4. Continuum convective regime

The continuum convective regime is defined by  $D \gg 1$ ,  $K \ll 1$ . Assuming that the velocity  $u_*$  and the mixing frequency  $\omega_m$  are the only relevant parameters, dimensional analysis then leads to the scalings  $S \sim 1$  and  $L \equiv \Delta \tilde{x} \sim 1/D$ . These scalings are

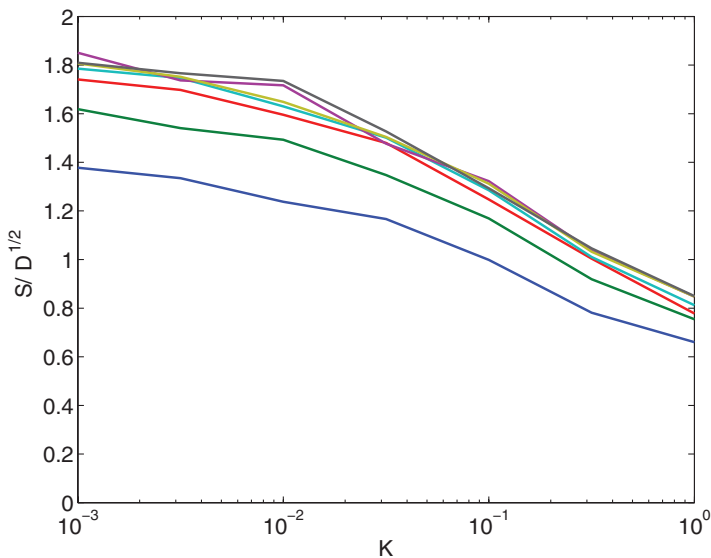


Figure 3. Scaled flame speed  $S/\sqrt{D}$  versus modelling Knudsen number  $K$  in the continuum diffusive regime. The curves (from bottom to top) are for Damkohler number  $D = 10^{-k/2}$  for  $k = 0, 1, \dots, 6$ .

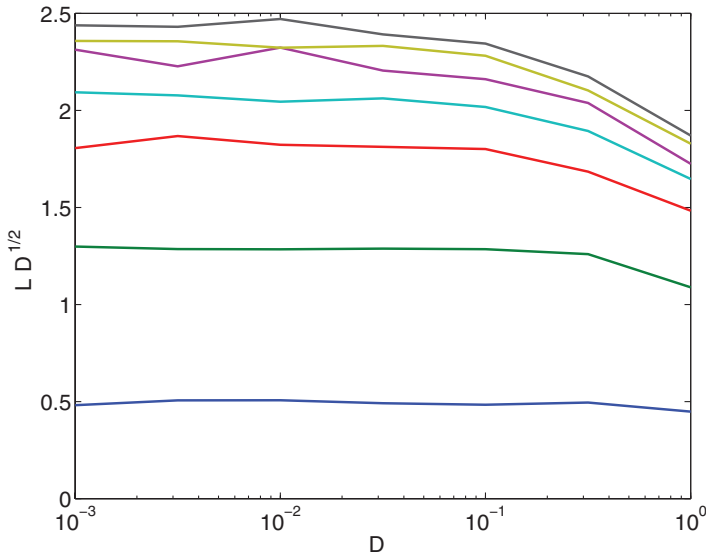


Figure 4. Scaled flame thickness  $L\sqrt{D}$  versus modelling Damkohler number  $D$  in the continuum diffusive regime. The curves (from bottom to top) are for Knudsen number  $K = 10^{-k/2}$  for  $k = 0, 1, \dots, 6$ .

investigated in Figures 9 and 10. As may be seen,  $S$  and  $DL$  become independent of  $D$  for  $D$  greater than 1000, say. However, as further examined in Figures 11 and 12, a weak dependence on  $K$  remains. Qualitatively these results are similar with the analysis of Section 4.

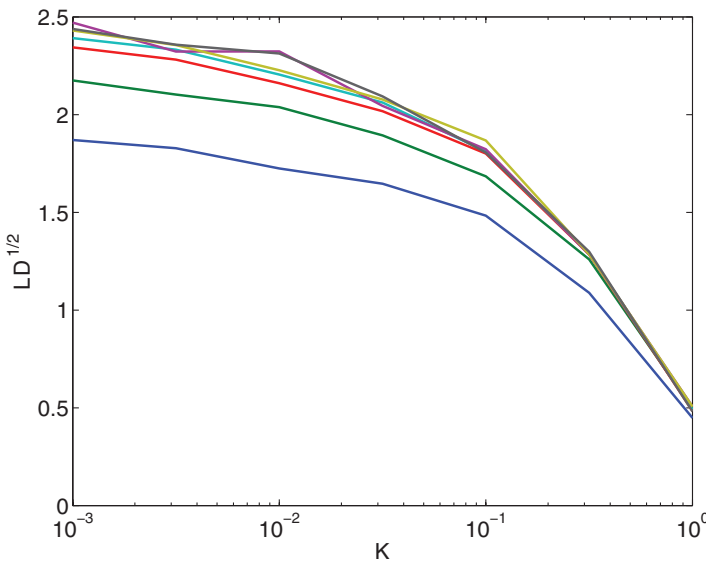


Figure 5. Scaled flame thickness  $L\sqrt{D}$  versus modelling Knudsen number  $K$  in the continuum diffusive regime. The curves (from bottom to top) are for Damkohler number  $D = 10^{-k/2}$  for  $k = 0, 1, \dots, 6$ .



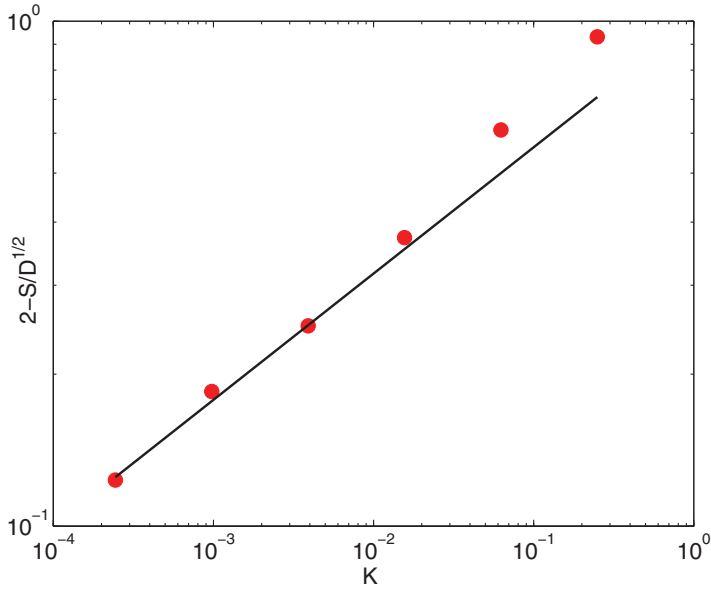


Figure 6. Variation with modelling Knudsen number of the departure of the flame speed from the Fisher–KPP value, for  $D = 2 \times 10^{-6}$ . The line is  $K^{1/4}$ .

In Figure 11, the lower and upper dashed lines show the estimated maximal propagation speed (Equation 66) for  $C_K = 1$  and  $C_K = 50$ , respectively. As may be seen, the observed speed  $S$  is very similar to  $u_{\max}(50/K)$ , and considerably larger than  $u_{\max}(1/K)$ . A large value of  $C_K$  may be related to the fact that the leading particle zone is asymptotically longer than the main transformation zone and thus contains more particles.

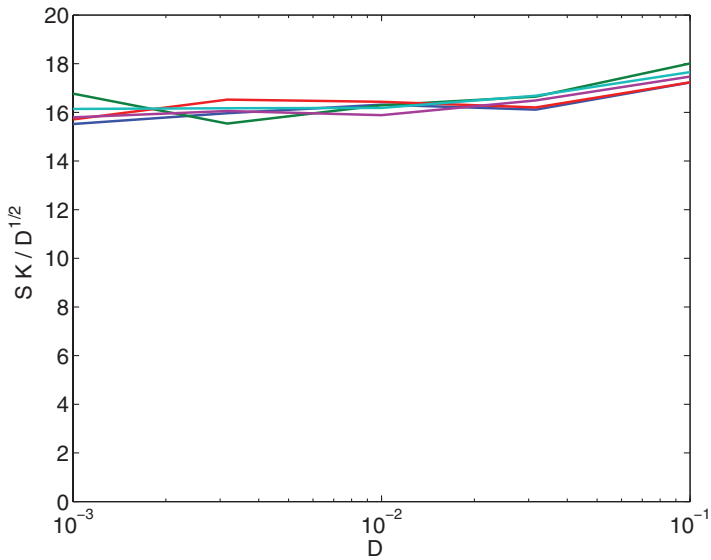


Figure 7. Scaled flame speed  $SK/\sqrt{D}$  versus modelling Damkohler number  $D$  in the rarefied diffusive regime. The curves are for Knudsen number  $K = 10^{k/2}$  for  $k = 3, 4, 5, 6$ .

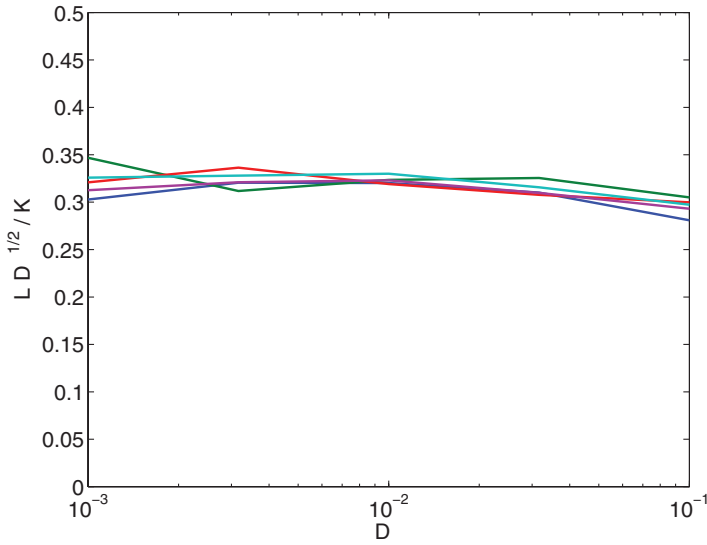


Figure 8. Scaled flame thickness  $L\sqrt{D}/K$  versus modelling Damkohler number  $D$  in the rarefied diffusive regime. The curves are for Knudsen number  $K = 10^{k/2}$  for  $k = 3, 4, 5, 6$ .

### 6. The convective regime $D_e \gg 1$ with phase-space localisation of mixing

In this section, the case of localisation of mixing in the phase (i.e.  $x-u$ ) space is considered. The distance  $x$  and velocity  $u$  are scaled by  $l_*$  and  $u_*$  for the purpose of localisation of mixing. Since localisation does not have much effect on the diffusive regime (see Section 3), only the convective regime (both continuum and rarefied) needs to be analysed

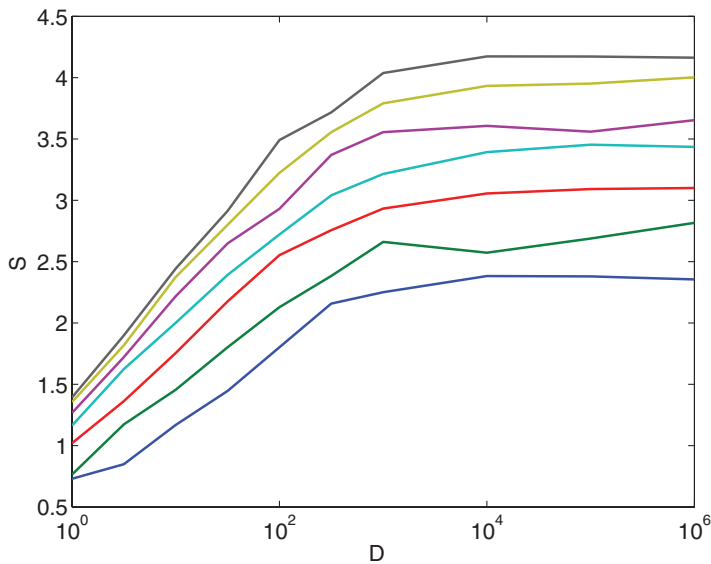


Figure 9. Normalised flame speed  $S$  versus modelling Damkohler number  $D$  in the continuum convective regime. The curves are for Knudsen number  $K = 10^{-k/2}$  for  $k = 0, 1, 2, 3, 4, 5, 6$ .

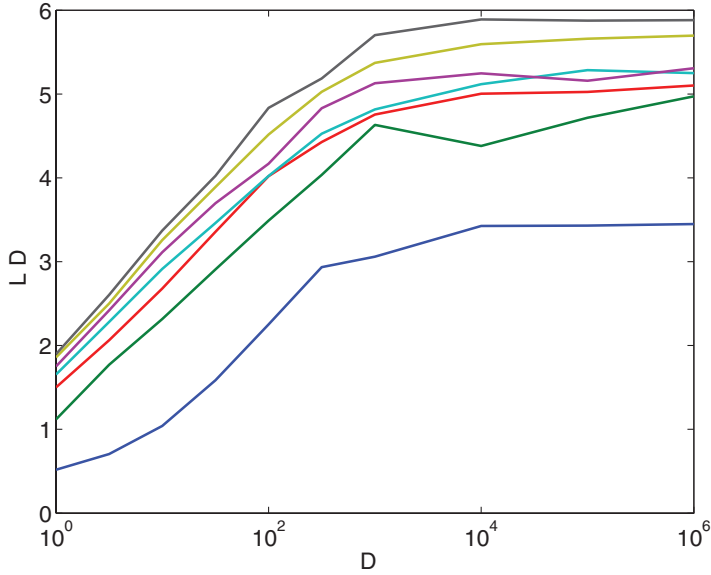


Figure 10. Scaled flame thickness  $LD$  versus modelling Damkohler number  $D$  in the continuum convective regime. The curves are for Knudsen number  $K = 10^{-k/2}$  for  $k = 0, 1, 2, 3, 4, 5, 6$ .

autonomously. Equation (30) is now written in the form

$$\frac{\partial \hat{g}}{\partial \tilde{t}} + U \frac{\partial \hat{g}}{\partial \tilde{x}} + U \frac{\partial \hat{g}}{\partial U} - \frac{\partial^2 \hat{g}}{\partial U^2} = -D_e \Omega \hat{h} \hat{g}, \tag{82}$$

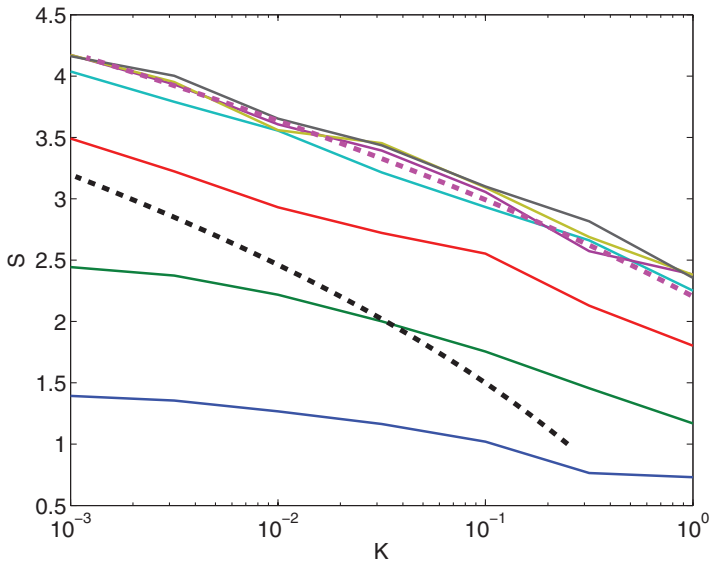


Figure 11. Normalised flame speed  $S$  versus modelling Knudsen number  $K$  in the continuum convective regime. The solid curves are for Damkohler number  $D = 10^k$  for  $k = 0, 1, 2, 3, 4, 5, 6$ . The lower and upper dashed lines are for  $\hat{u}_{\max}(1/K)$  and  $\hat{u}_{\max}(50/K)$ , respectively.

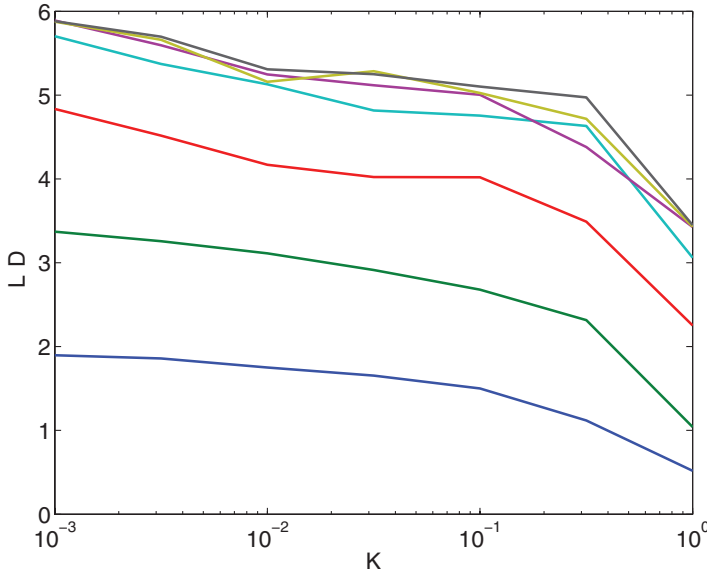


Figure 12. Scaled flame thickness  $LD$  versus modelling Knudsen number  $K$  in the continuum convective regime. The curves are for Damkohler number  $D = 10^k$  for  $k = 0, 1, 2, 3, 4, 5, 6$ .

or equivalently

$$\frac{\partial \hat{h}}{\partial \tilde{t}} + U \frac{\partial \hat{h}}{\partial \tilde{x}} + U \frac{\partial \hat{h}}{\partial U} - \frac{\partial^2 \hat{h}}{\partial U^2} = D_e \Omega \hat{h} \hat{g}, \tag{83}$$

where

$$\tilde{t} = \frac{t}{\tau_*}, \quad \tilde{x} = \frac{x}{\tau_* u_*}, \quad U = \frac{u}{u_*}, \quad D_e = 2w_0 \tau_*,$$

and, generally,  $\Omega = \Omega(U)$ . With the use of Lagrangian time

$$\frac{\partial}{\partial \tilde{t}^\circ} = \frac{\partial}{\partial \tilde{t}} + U \frac{\partial}{\partial \tilde{x}}$$

we can write

$$\frac{\partial \hat{h}}{\partial \tilde{t}^\circ} + U \frac{\partial \hat{h}}{\partial U} - \frac{\partial^2 \hat{h}}{\partial U^2} = D_e \Omega \hat{h} \hat{g}, \tag{84}$$

where  $\hat{g} = 1 - \hat{h}$ . When  $D_e \rightarrow \infty$ , the steady wave solution of Equation (84) is represented by a thin (in velocity space) flame  $\Delta U \sim D_e^{-1/2}$ . The flame position in velocity space is denoted by  $U_f(\tilde{t}^\circ)$  and we introduce  $\tilde{v} = U - U_f$ . At the leading order, the flame is then controlled by the KPP–Fisher equation

$$-A \frac{\partial \hat{h}}{\partial \tilde{v}} - \frac{\partial^2 \hat{h}}{\partial \tilde{v}^2} = D_e \Omega(U_f) \hat{h} (1 - \hat{h}),$$

where  $A = U_f| - dU_f|/d\tilde{r}^\circ$ . This equation represents the steady wave form of the KPP–Fisher Equation (3) with the propagation speed  $A$  in the velocity space given by (compare with Equation 4)

$$A(U_f|) = 2\sqrt{D_e\Omega(U_f|)}.$$

Note that the minimal speed is selected here in accordance with the KPP theory. The definition of  $A$  can now be rewritten as a differential equation for the flame position in the velocity space

$$\frac{dU_f|}{d\tilde{r}^\circ} = U_f| - A(U_f|).$$

In a steady wave propagating in the physical space with normalised velocity  $S$  the Lagrangian derivative is given by

$$\frac{dU_f|}{d\tilde{r}^\circ} = (U_f| - S)\frac{\partial U_f|}{\partial \tilde{x}} = U_f| - A(U_f|). \quad (85)$$

Solvability of this equation requires that  $U_f| = A(U_f|)$  when  $U_f| = S$ , hence  $S = A(S)$  or

$$S = 2\sqrt{D_e\Omega(S)}. \quad (86)$$

Note that  $A(U)$  is either constant or a decreasing function of  $U$ , and so  $A(U) = U$  has only a single solution. Equation (85) can be integrated to determine the location of the flame front in phase space: if  $A$  is constant, the flame is located on a straight line.

### 6.1. Rarefied regime

In this case the effective mixing frequency is determined by the collision frequency  $\omega_e = \omega_c$ . The collision frequency is inversely proportional to the mean square distance between particles, which, in two-dimensional  $x-u$  space, is inversely proportional to the concentration of Pope particles. Hence we can write according to (45)

$$\omega_e = \omega_c(U) = \omega_{c0} \exp\left(-\frac{U^2}{2}\right).$$

With  $\omega_e = \omega_{c0}$ , Equation (86) takes the form

$$S = 2\sqrt{D_c \exp\left(-\frac{S^2}{2}\right)}. \quad (87)$$

The leading order approximation of this equation is given by the estimate

$$D_c \exp\left(-\frac{S^2}{2}\right) \sim 1,$$

yielding

$$\frac{s}{u_*} = S \sim \sqrt{C_2 + 2 \ln(D_c)} = \sqrt{C_2 + 2 \ln(2\omega_{c0}\tau_*)}. \quad (88)$$

Note the similarity with Equation (73) although the constants  $C_1$  and  $C_2$  may be different. According to (45), the leading order term for the speed is given by  $S^2 \sim \ln(R)$ .

### 6.2. Continuum regime

In this case the effective mixing frequency is determined by the mixing rate  $\omega_e = \omega_m = \text{const}$  and  $\Omega = 1$ . Hence Equation (86) takes the form

$$\frac{s}{u_*} = S = 2D^{1/2} = 2\sqrt{2\omega_m\tau_*}. \quad (89)$$

Note the similarity with Equation (56). The speed  $S = 2D^{1/2}$  specified by Equation (89) cannot exceed the speed  $S^2 \sim \ln(R)$  predicted by (88). When the continuum case is observed at  $u \sim u_*$ , the situation at the fringes  $u \sim s \gg u_*$  may still be rarefied and the fringes control the propagation speed by Equation (88). Hence the transition between the power law and logarithmic regimes occurs at the line specified by  $4D \sim \ln(R)$  or  $R \sim \exp(4D)$  and not at the line  $D_c \sim 1$  as in the case of the physical-space localisation of mixing. This point is illustrated in Figure 1, which shows the location of the line  $R \sim \exp(4D)$  on the regime diagram. Note that the phase-space localisation of mixing extends the power-law dependence  $s \sim D^{1/2}$  from the diffusive to the convective regimes, which is not the case for the localisation of mixing in physical space where the convective regime corresponds to the logarithmic dependence (72) of  $s$  on  $D$ .

### 7. How fast can we burn?

First we note that in the diffusional regime ( $D_c \ll 1$ ) the burning velocity (56) is typically well below  $u_*$ . Although Equation (56) is consistent with the Damkohler limit  $s/u_* \sim \text{Da}^{1/2}$  as  $\text{Da} \rightarrow 0$  [29] assuming that the mixing frequency is linked to the reaction rate by  $\omega_m = 1/\tau_r$  (note that  $\omega_m = 1/\tau_r$  is used only for small  $\text{Da}$ ) this behaviour is a general property of the diffusion–reaction equations and does not indicate that the reaction source term can be (or needs to be) incorporated into competitive mixing as in the present model. In this section, we continue using  $s$  for the turbulent flame speed and  $u_*$ ,  $l_*$  and  $\tau_*$  for the corresponding macro-scales of turbulence. Here, we are interested in the question of maximal wave speeds and these speeds  $s/u_* = S \gtrsim 1$  are achieved in the convective regime. We note that, for both localisations considered here, the wave speed is restricted by the equation  $S^2 \lesssim \ln(R)$ . This restriction indicates that there should be a sufficient number of particles that move with velocity  $u \sim s$ , otherwise there would not be a sufficient number of agents that can carry the wave front forward at speed  $s$ . The number of particles decreases exponentially with increasing  $u$ , imposing this constraint on the speed  $s$ .

We now consider the speed of propagation of turbulent premixed flames while leaving aside the effects of the Lewis and Markstein numbers. Bradley *et al.* [30] suggested that the Karlovitz number  $\text{Ka}$  is the key parameter that can be used for parametrisation of turbulent premixed burning velocities. Since the definition of the  $\text{Ka}$  number is based on the Kolmogorov scales of turbulence, the importance of  $\text{Ka}$  implies that Kolmogorov

scaling of turbulence is not changed by the flame even in the vicinity of the flame. This assumption is not trivial since the complex interaction of density and viscosity jumps and turbulence may, in principle, alter the fundamental properties of turbulence. If the flame velocities have the same scaling as turbulence and the fluctuations of the smallest scales are represented by Kolmogorov quantities, we can write

$$\frac{s}{u_*} \sim \frac{s_L}{u_K} \sim \text{Ka}^{-1/2}, \quad (90)$$

where  $s_L$  is the laminar flame speed and the subscript ‘K’ is used to indicate Kolmogorov scales. Here, we assume that burning velocities associated with different scales follow the conventional turbulent cascade. Equation (90) does not approximate experimental data particularly well overestimating the dependence of  $s$  on  $\text{Ka}$ . This apparent discrepancy can be explained by the effect of flame-generated turbulence. At large scales, flame propagates in intrinsic turbulence while at the smallest scales flame propagates in both intrinsic turbulence and turbulence generated by flame (here we consider the generation of large-scale fluctuations by alterations of the flame speed and direction and not the small-scale fluctuations generated by flame instabilities which exist in a laminar flame). The flame-generated turbulence would affect the value of the Kolmogorov scales, specifically  $u_K$  needs to be replaced by the effective Kolmogorov scale, which can be estimated as  $u_K^\circ \sim u_K (u_*^\circ/u_*)^{3/4}$  where  $u_*^\circ$  is the new effective large-scale intensity of turbulence. Here we take into account that  $u_K \sim u_* \text{Re}^{-1/4}$  and  $u_K^\circ \sim u_*^\circ (\text{Re}^\circ)^{-1/4}$ , where the effective Reynolds number is specified by  $\text{Re}^\circ \sim (u_*^\circ/u_*) \text{Re}$  implying that the integral length scale of turbulence  $l_*$  does not change. Assuming that flame-generated turbulence is dominant we estimate  $u_*^\circ \sim s$ , substitute  $u_K^\circ$  for  $u_K$  in (90) and obtain the ‘4/7 power law’ suggested by Klimenko [31]

$$\frac{s}{u_*} \sim \frac{s_L}{u_K^\circ} \sim \frac{s_L}{u_K} \left( \frac{u_*}{s} \right)^{3/4},$$

that is  $s/u_* \sim (s_L/u_K)^{4/7}$  and

$$\frac{s}{u_*} = a \left( \frac{\text{Da}}{\text{Re}^{1/2}} \right)^b \sim \text{Ka}^{-b}, \quad b = 2/7. \quad (91)$$

This dependence is strongly supported by experimental evidence: with  $a = 1.5$  Equation (91) produces a very good match for the data correlation by Bradley *et al.* [30], who suggested an empirical value of  $b = 0.3$ . Conventional representations of the flame propagation velocity  $s$  in terms of the parameters of the laminar flame and turbulence are not affected by a small change in  $b$  and are consistent with [30]. Lipatnikov and Chomiak [19] determined that other experimental databases for turbulent premixed flames are consistent with the results in [30]: the value of  $b$  typically falls within the range of  $1/4 \leq b \leq 1/3$ , although the largest detected value of  $b$  was anomalously high ( $b = 0.44$ , as can be inferred from [19]).

If the Reynolds number  $\text{Re}$  is large, approximation (91) allows for  $s \gg u_* \gg s_L \gg u_K$  raising questions about how the leading points in the flame can move with the speed  $s$  if all other velocities in the flow are much smaller. Probabilities of large velocity fluctuations are exponentially small and the top velocities are likely to be restricted by  $\ln(\text{Re})$ . Hence, it is possible that the asymptote given by (91) is intermediate and, for large  $\text{Re}$ , the flame speed may be restricted by logarithmic terms which can be relevant to the logarithmic

terms obtained in the present work. We note that the theory suggested by Kuznetsov and Sabelnikov [16] explicitly predicts logarithmic dependence of the effective propagation speed on  $Re$ . The data of Bradley *et al.* [30] indicate that  $s/u_*$  can be of the order of 10 and still compliant with (91), although the  $Re$  number is not particularly high for these cases.

The model under consideration needs specification of the rate of competitive mixing  $\omega_m = \tau_m^{-1}$ . Application of the hypothesis of Kolmogorov cascade to  $\omega_m$  indicates that

$$\tau_m \sim \tau_r \frac{\tau_*}{\tau_K}, \tag{92}$$

since mixing is determined by large-scale processes while in the flamelet regime the chemical reactions are linked to the processes at the smallest (Kolmogorov) scales. Substitution of this hypothesis into Equations (73) and (89) results in  $s^2/u_*^2 \sim \ln(Ka^{-1}) + \text{const}$  and  $s/u_* \sim Ka^{-1/2}$  correspondingly. Note that here we consider only continuum regimes and presume that a sufficient number of particles is present in the simulations. The model based on localisation of mixing in physical space significantly underpredicts the dependence of  $s$  on  $Ka$  while the model based on localisation in the phase space is consistent with (90). The effects of flame-generated turbulence can be taken into account by replacing  $\tau_K$  in (92) by the effective Kolmogorov time  $\tau_K^\circ = l_K^\circ/u_K^\circ$

$$\tau_m \sim \tau_r \frac{\tau_*}{\tau_K^\circ} \sim \tau_r \frac{\tau_*}{\tau_K} \left( \frac{s}{u_*} \right)^{3/2}, \tag{93}$$

where the effective Kolmogorov scale is given by  $l_K^\circ \sim (u_*/s)^{3/4} l_K$  assuming, as in the derivation of (91), that the length macroscale does not change  $l_*^\circ \sim l_*$  and  $u_K^\circ \sim u_K(u_*^\circ/u_*)^{3/4}$ . When the approximation of  $s$  specified by (91) is used in Equation (93), this equation relates the value of modelling scale  $\tau_m$  to turbulence and reaction scales. This determines the value of the modelling Damkohler number  $D$ , which is not to be confused with the physical Damkohler number  $Da$ . Substitution of scaling (93) into Equation (89) results in  $s/u_* \sim Ka^{-2/7}$  (and in  $\omega_m \sim \tau_*^{-1} Ka^{-4/7}$ ) coinciding with the ‘4/7 power law’ specified by (91) and producing a very good match for the speeds of turbulent premixed flames observed in experiments. It should be noted, however, that the present model is a constant-density model – it does not simulate directly turbulence generated by flame but simply allows for enforcing of scaling induced by this process.

The present consideration may also be relevant to the fact that traditional invasion theory based on the KPP–Fisher equation may grossly underestimate the speed of invasion observed in some cases. For example, the very fast rate of invasion of plant species after the onset of the current interglacial period is known as the Reid paradox (see Clark *et al.* [32]), which was discovered by Clement Reid more than a hundred years ago. Without drawing any conclusions, we note that velocities associated with movements of species can have many components of different magnitudes and with different correlation times. The existence of longer correlations can, as discussed in the present work, significantly contribute to faster propagation of the species.

### 8. Conclusions

The particles with random walk, properties and mixing – the Pope particles – can be used to simulate various realistic processes stochastically. Pope particles with competitive mixing give an alternative stochastic formulation for the model specified by the KPP–Fisher



equation – this equation is conventionally used to model invasions, simple epidemics and the propagation of turbulent premixed flames (the BML model). The present work focuses on the effects of finite correlation time of particle motions and considers two types of localisation of competitive mixing: localisation in physical ( $x$ ) space and localisation in the phase ( $x-u$ ) space. Changes between continuum and rarefied regimes, which is determined by the number of particles used in simulations, is considered. Major asymptotes for the propagation speed of steady waves are analysed and stochastic simulations confirming the analysis are performed.

When the correlation time is small (the diffusive regime), the model is shown to reproduce the KPP–Fisher equation at the leading order. When the correlation time is large (the convective regime), the model behaviour depends on localisation: phase-space localisation of mixing tend to produce faster propagation speeds. A summary of the computational regimes is given in Appendix B. With the mixing frequency that follows scaling derived from the ‘4/7 power law’, the model based on the phase-space localisation of mixing produces results that are consistent with existing experimental evidence for the propagation speed of turbulent premixed flames in the flamelet regime. Simulations based on the physical-space localisation can be expected to underestimate the propagation speed for this regime.

### Acknowledgement

The work of AYK is supported by the Australian Research Council. The work of SBP was supported in part by the Air Force Office of Scientific Research under grant FA-9550-09-1-0047 and in part by the Department of Energy under grant DE-FG02-90ER14128.

### References

- [1] S.B. Pope and M.S. Anand, *Flamelet and distributed combustion in premixed turbulent flames*, Proc. Combust. Inst. 20 (1985), pp. 403–410.
- [2] A.Y. Klimenko and M.J. Cleary, *Convergence to a model in sparse-Lagrangian fdf simulations*, Flow Turbul. Combust. 85 (Special Issue dedicated to S.B. Pope) (2010), pp. 567–591.
- [3] S.B. Pope, *PDF methods for turbulent reactive flows*, Prog. Energy Combust. Sci. 11 (1985), pp. 119–192.
- [4] A.Y. Klimenko, *Conservative and competitive mixing and their applications*, Phys. Scripta T142 (2010), 014054. doi:10.1088/0031-8949/2010/T142/014054
- [5] K.N.C. Bray, P.A. Libby, and J.B. Moss, *Flamelet crossing frequencies and mean reaction rates in premixed turbulent combustion*, Combust. Sci. Technol. 41 (1984), pp. 143–172.
- [6] C. Dopazo, *Recent developments in PDF methods*, in *Turbulent Reacting Flows*, P.A. Libby and F.A. Williams, eds., Chap. 7, Academic Press, London, 1994, pp. 375–474.
- [7] S.B. Pope, *Turbulent Flows*, Cambridge University Press, Cambridge, UK, 2000.
- [8] R. Fox, *Computational Models for Turbulent Reacting Flows*, Cambridge University Press, Cambridge, UK, 2003.
- [9] S. Heinz, *Statistical Mechanics of Turbulent Flows*, Springer-Verlag, Berlin, 2003.
- [10] H. Pitsch, *Large-eddy simulations of turbulent combustion*, Annu. Rev. Fluid Mech. 38 (2006), pp. 453–482.
- [11] D. Haworth, *Progress in probability density function methods for turbulent reacting flows*, Prog. Energy Combust. Sci. 36 (2010), pp. 168–259.
- [12] F.A. Williams, *Combustion Theory*, 2nd ed., Addison-Wesley, Reading, MA, 1985.

- [13] Ya.B. Zeldovich, G.I. Barenblatt, V.B. Librovich, and G.M. Makhviladze, *The Mathematical Theory of Combustion and Explosions*, Consultants Bureau, New York, 1985.
- [14] F.C. Gouldin, *An application of fractals to modeling premixed turbulent flames*, Combust. Flame 68 (1987), pp. 249–266.
- [15] S.B. Pope, *Turbulent premixed flames*, Annu. Rev. Fluid Mech. 19 (1987), pp. 237–270.
- [16] V.R. Kuznetsov and V.A. Sabelnikov, *Turbulence and Combustion*, Hemisphere, New York, 1990.
- [17] D. Bradley, *How fast can we burn?* Proc. Combust. Inst. 24 (1992), p. 247.
- [18] N. Peters, *Turbulent Combustion*, Cambridge University Press, Cambridge, UK, 2000.
- [19] A. Lipatnikov and J. Chomiak, *Turbulent flame speed and thickness: Phenomenology, evaluation, and application in multi-dimensional simulations*, Prog. Energy Combust. Sci. 28 (2002), pp. 1–73.
- [20] A.G. Class, B.J. Matkowsky, and A.Y. Klimenko, *Stability of planar flames as gasdynamic discontinuities*, J. Fluid Mech. 491 (2003), p. 51.
- [21] R.A. Fisher, *The wave of advance of advantageous genes*, Ann. Eugen. 7 (1937), p. 355.
- [22] A.N. Kolmogorov, I.G. Petrovsky, and N.S. Piskunov, *A study of the equation of diffusion with increase in the quantity of matter, and its application to a biological problem*, Mosc. Univ. Bull. A: Math. Mech. 1 (1937), p. 1.
- [23] D. Mollison, *Spatial contact models for ecological and epidemic spread*, J. R. Statist. Soc. B 39 (1977), p. 283.
- [24] H.P. McKean, *Application of Brownian motion to the equation of Kolmogorov–Petrovskii–Piskunov*, Comm. Pure Appl. Math. 28 (1975), pp. 323–331.
- [25] R.A. Blythe and A.J. McKane, *Stochastic models of evolution in genetics, ecology and linguistics*, J. Statist. Mech.: Theor. Exp. 2007 (2007), P07018. doi:10.1088/1742-5468/2007/07/P07018
- [26] A.Y. Klimenko, *Lagrangian particles with mixing – I: Simulating scalar transport*, Phys. Fluids 21 (2009), 065101. doi:10.1063/1.3147925
- [27] P. Jenny and B. Rembold, *Modeling interaction of turbulence with premixed combustion using a joint PDF approach*, First International Conference on Turbulence and Interactions (TI2006), ONERA France, Porquerolles, France, 2006.
- [28] A.Y. Klimenko and R.W. Bilger, *Conditional moment closure for turbulent combustion*, Prog. Energy Combust. Sci. 25 (1999), pp. 595–687.
- [29] G. Damkohler, *Der Einfluss der Turbulenz auf die Flammengeschwindigkeit in Gasgemischen*, Z. Elektrochem. 46 (1940), pp. 601–626.
- [30] D. Bradley, A.K.C. Lau, and M. Lawes, *Flame stretch rate as a determinant of turbulent burning velocity*, Phil. Trans. R. Soc. Lond. A 338 (1992), pp. 359–387.
- [31] A.Y. Klimenko, *Examining the cascade hypothesis for turbulent premixed combustion*, Combust. Sci. Tech. 139 (1998), pp. 15–40.
- [32] J.S. Clark, C. Fastie, G. Hurtt, S.T. Jackson, C. Johnson, G.A. King, M. Lewis, J. Lynch, S. Pacala, C. Prentice, E.W. Schupp, T. Webb (III), and P. Wyckoff, *Reid’s paradox of rapid plant migration*, Biosci. 48 (1998), p. 13.
- [33] M.D. Donsker, *An invariance principle for certain probability limit theorems*, Mem. Amer. Math. Soc. 6 (1951), p. 12.
- [34] B. Kjos-Hanssen and T. Szabados, *Kolmogorov complexity and strong approximation of Brownian motion*, Proc. Amer. Math. Soc. 139(9) (2011), pp. 3307–3316.
- [35] E.A. Asarin, *Individual random signals: An approach based on complexity*, Ph.D. diss., Moscow University, 1988.

### Appendix A. Brownian relay

In this section we consider the speed of propagation of disturbances by a large number of Brownian particles (or Wiener processes) whose distribution along coordinate  $x$  is statistically uniform. Particle markers can be relayed from one particle to another when their trajectories intersect selecting the particle that progresses forward faster, i.e. leads after the intersection. The propagation speed of the marker (that is of the leading marked particle) is the quantity of interest. The average distance between the particles is  $l_p$  and the diffusion coefficient of particle random walk is  $\mathfrak{D}$ . Dimensional arguments result in the following equation for the propagation speed:

$$s = C_0 \frac{\mathfrak{D}}{l_p}, \quad (\text{A1})$$

where  $C_0$  is a constant. This equation is consistent with Equation (57). The variance of the flame position is expected to increase with time. The particles can relay information to each other only when their trajectories intersect. ‘Brownian relay’ corresponds to competitive mixing with two states  $Y = 0$  and  $Y = 1$  among Pope particles that randomly walk in a single dimension  $x$ . Mixing, which is specified by the rules specified in Table 1, is fully localised and occurs when and only when particle trajectories intersect. If at time  $t$  the particles are segregated so that  $Y = 1$  for all particles with  $x \leq x_f(t)$  and  $Y = 0$  for all particles with  $x > x_f(t)$ , this segregation persists at future times. The identity of the leading particle – the rightmost particle with  $Y = 1$  located at  $x = x_f(t)$  – changes when it is overtaken by another  $Y = 1$  particle from the left or possibly when it intersects with another particle from the right which immediately converts from  $Y = 0$  to  $Y = 1$ . The purpose of the present analysis is to determine the constant  $C_0$ . Brownian relay can be considered as the limit of a simple random walk. Let  $n_p$  particles be distributed between  $n_b$  bins; each bin has a size of  $\Delta x_b$  so that

$$l_p = \Delta x_b \frac{n_b}{n_p}. \quad (\text{A2})$$

At each time step  $\Delta t$  each particle moves right or left one bin with equal probability and independently of anything else. The diffusion coefficient associated with this random walk is

$$\mathfrak{D} = \frac{1}{2} \frac{\Delta x_b^2}{\Delta t} \quad (\text{A3})$$

since the variance of particle positions is increased by  $\Delta x_b^2$  every time step. The discrete random walk converges to Brownian trajectories with the diffusion coefficient  $\mathfrak{D}$  at the limit  $\Delta x_b, \Delta t \rightarrow 0$ , preserving the value of  $\mathfrak{D}$  in (A3). While a weak convergence (i.e. convergence of probability distributions) follows from the Central Limit and Donsker theorems [33], we need a stronger version of the convergence theorem – the result that was recently proved by Kjos-Hanssen and Szabados [34] and represents strengthening of the conditions of the Asarin theorem [35]. The strong convergence theorem [34] demonstrates a strong, almost sure convergence of the simple random walk to Brownian paths and the rate of convergence is given by  $(\Delta x)_{n_s} \sim (n_s)^{-1/2} \ln(n_s)$ , where  $(\Delta x)_{n_s}$  is the deviation of the random walk approximation from the Brownian trajectory and  $n_s = t_s/\Delta t$  is the number of time steps defined as the length of the time interval under consideration  $t_s$  divided by  $\Delta t$ . We assume that all particles are initially distributed between even bins with equal

probability. In this case, only odd bins can be occupied by particles at odd time steps and only even bins can be occupied at even time steps. The discrete trajectories of particles can intersect only if two particles are in the same bin at one of the time steps. Without loss of generality, we assume that the relay propagates from left to right. We call the rightmost (maximal  $x$ ) particle(s) with  $Y = 1$  ‘the leading particle(s)’ and the bin where the leading particle(s) are located is ‘the leading bin’. There could be one or more leading particles but there is only one leading bin. All particles to the left of the leading bin have  $Y = 1$  while all particles to the right of the leading bin have  $Y = 0$ . The number of bins and number of particles must be large to investigate the propagation speed. In addition we use  $n_b \gg n_p$ , so that  $p_b \equiv n_p/(n_b/2) \ll 1$  is the bin selection probability since either even or odd bins are occupied at every time step. At every time step, particles are randomly distributed between the even or odd bins and probabilities of having  $k$  particles in a bin is given by the Poisson distributions  $p_k = p_b^k e^{-p_b}/k!$ . Hence, on average  $p_0 \approx 1 - p_b + p_b^2/2$  bins do not have particles,  $p_1 \approx p_b - p_b^2$  bins have a single particle and  $p_2 \approx p_b^2/2$  bins have two particles. The probability of having three  $p_3 \approx p_b^3/6$  or more particles is neglected as  $p_b$  is small. This leads to vanishing probability of simultaneous multiple intersections. The total number of bins  $n_b(p_0 + p_1 + p_2) = n_b$  and total number of particles  $n_b(p_1 + 2p_2) = n_b p_b = n_p$  are as expected. The leading bin by definition has at least one particle, hence it has one particle with probability  $p_{b1} \equiv p_1/(p_1 + p_2) \approx 1 - p_b/2$  and two particles with probability  $p_{b2} \equiv p_2/(p_1 + p_2) \approx p_b/2$ . If the leading bin has one particle, then the next position of the leading bin is its either right or left neighbours with probability 50%. If the leading bin has two particles, then there are four equally probable possibilities for the particles from the bin to be distributed between the left and right bin neighbours. The particle with larger  $x$  is then selected as the leading particle. Hence in three cases the leading bin moves right and only in one case it moves left. The average drift velocity for this event is  $\Delta x_b/(2\Delta t)$ . Multiplication by the event probability  $p_{b2}$  yields the expression for the leading bin speed

$$s = p_{b2} \frac{\Delta x_b}{2\Delta t} = \frac{n_p}{n_b} \frac{\mathcal{D}}{\Delta x_b} = \frac{\mathcal{D}}{l_p}, \tag{A4}$$

that is  $C_0 = 1$  in (A1). This result has been confirmed by stochastic simulations. The limit of  $\Delta x_b, \Delta t \rightarrow 0$ , and  $n_b, n_s \rightarrow \infty$ , so that  $\mathcal{D} = \text{const}$ ,  $n_p = \text{const}$ ,  $t_s = \text{const}$  and  $l_p = \text{const}$  converges to the process of Brownian relay. While convergence to the Brownian trajectories is discussed above, the convergence of the trajectories’ property of intersecting each other needs some remarks. In a given time interval (fixed or randomly selected but not linked to first or last intersection time), two Brownian particle trajectories (i.e. two Wiener processes) are almost surely either separated by a finite gap or have a finite overlap. The situation of two trajectories just touching each other (in a fixed time interval or before the moment of intersecting with a third trajectory) is geometrically possible but has zero probability. Hence for any two trajectories, as the deviation  $(\Delta x)_{n_s}$  becomes much smaller than the gap or overlap (and  $\Delta t$  becomes shorter than the overlap duration) the property of intersecting or not intersecting becomes fixed in the converging sequence.

It is interesting that although the characteristic effective collision frequency is given by the estimate  $\omega_c \sim \mathcal{D}/l_p^2$ , the actual number of collisions (i.e. intersections of Brownian trajectories) become infinite. Indeed, the probability of this event at each time step is  $p_{b2} \sim s\Delta t/\Delta x_b$  while there are  $\sim 1/\Delta t$  steps; hence the number of intersection events is  $\sim p_{b2}/\Delta t \sim s/\Delta x_b \rightarrow \infty$  as  $\Delta x_b \rightarrow 0$ . This agrees with a known property of Brownian trajectories: they either do not intersect in an interval or they have an infinite number of intersections in that interval. Note that  $C_0 = 1$  only if the particles can relay information to

Table B1. Summary of the major scales and parameters.

$\tau_*$	Velocity convection time scale
$\tau_m \equiv 1/\omega_m$	Mixing time scale
$\tau_p \equiv l_p/u_*$	Particle time scale
$\tau_c = \begin{cases} \tau_p & R \gg 1 \\ \frac{1}{2} \frac{\tau_p^2}{\tau_*} & R \ll 1 \end{cases}$	Collision time scale
$\tau_e = \max(\tau_m, \tau_c)$	Effective mixing time scale
$D \equiv 2\tau_*/\tau_m$	Modelling parameter resembling the Damkohler number
$R \equiv (\tau_*/\tau_p)^2 = (u_*\tau_*/l_p)^2$	Modelling parameter resembling the Reynolds number

each other only when their trajectories intersect. If information exchanges were allowed at finite distances, the speed  $s$  would be faster and this would increase  $C_0$  so that it becomes dependent on the details of the mixing process.

**Appendix B. Summary of the major parameters and regimes**

There are three major time scales in the problem, i.e.  $\tau_*$ ,  $\tau_m$  and  $\tau_p$ , which form two independent dimensionless parameters  $D$  and  $R$ . These time scales and parameters are specified in Table B1. The other dimensionless parameters (such as  $K$ ) depend on  $D$  and  $R$ .

We also introduce the effective mixing time  $\tau_e$  and the collision time  $\tau_c$  which are determined by the major time scales  $\tau_*$ ,  $\tau_m$  and  $\tau_p$ . If  $\tau_m \ll \tau_c$ , then it is the collision time  $\tau_c$  that determines the effective mixing rate. This property is utilised by introducing the effective mixing time  $\tau_e$ , although we note that replacement of  $\tau_m$  by  $\tau_c$  is approximate and the effective mixing rate between particles may depend on the particulars of the mixing scheme. The relative values of the three time parameters imply six different possibilities that are reduced to four different regimes summarised in Table B2.

The main regimes are denoted in the table as: R – Rarefied, C – Continuum, V – conVec-tive, D – Diffusive; and modifiers ‘x’ and ‘xu’ indicate localisation of mixing. The regime diagram is shown in Figure 1. These regimes are investigated in the following sections:

- CD – continuum diffusive: asymptote represented by KPP–Fisher equation (Section 3);
- RD – rarefied diffusive: approximate application of the CD solution (Section 3) and Brownian relay (Appendix A);
- CVx – continuum convective with  $x$ -space localisation (Section 4);
- RVx – rarefied convective with  $x$ -space localisation (Section 4);
- CVxu – continuum convective with phase-space localisation (Section 6);
- RVxu – rarefied convective with phase-space localisation (Section 6).

Table B2. Summary of the regimes.

Case	Expression for $\tau_c$	$x$ -localisation	$x-u$ -localisation
$\tau_m < \tau_* < \tau_c$	I	RD	RD
$\tau_* < \tau_m < \tau_c$	I	RD	RD
$\tau_* < \tau_c < \tau_m$	I	CD	CD
$\tau_c < \tau_* < \tau_m$	II	CD	CD
$\tau_c < \tau_m < \tau_*$	II	CVx	CVxu
$\tau_m < \tau_c < \tau_*$	II	RVx	RVxu

Downloaded by [Cornell University] at 12:20 18 August 2012